N73-20721
NASA CR-112206
CASE FILE Cy.

PERFORMANCE EVALUATION OF A STRAPDOWN ELECTRICALLY SUSPENDED GYRO FOR SPACE

by

Donald F. Elwell

John C. Wacker

James M. Miletich

March 1973

Prepared under Contract No. NAS 1-11078 by

HONEYWELL INC.
Aerospace Division
St. Petersburg, Florida

for

NATIONAL AERONAUTICS AND SPACE ADMINISTRATION

FOREWORD

This report presents the results of a Performance Evaluation of a Strapdown Electrically Suspended Gyro which is intended for space applications. The work was performed under National Aeronautics and Space Administration Contract No. NAS 1-11078.

The program was devoted to the improvement in readout accuracy of the type of strapdown Electrically Suspended Gyro which employs a set of electro-optical pickoffs viewing a line pattern on the gyro rotor. The principal program effort was directed toward improvement of pattern line edge accuracy because errors in edge placement are the major source of readout error. Readout accuracy test results on the complete gyro are reported.

Honeywell Inc., Aerospace Division, performed the program under the technical direction of Principal Investigator Donald F. Elwell. The program was conducted from 2 September 1971 to 15 November 1972.

Acknowledgment is extended to the Spectra-Physics Corporation of Mountain View, California, for their contribution to the program through the loan of the Helium-Cadmium Laser utilized in all of the photoresist patterning experiments.

Gratitude is extended to NASA Langley Research Center, for their technical guidance, under the program technical direction of Mr. Gordon Bullock.

TABLE OF CONTENTS

	Page
FOREWORD	iii
List of Illustrations	v
List of Tables	vi
SUMMARY	1
INTRODUCTION	2
PATTERN APPLICATION DEVELOPMENT	3
Pattern Analysis	3
Rotor Surface Treatment	15
Laser Photoresist Method	18
Patterning By Surface Abrasion	26
GYRO MODIFICATION	33
Rotor Fabrication and Selection	33
Readout Electronics Modification	33
GYRO ASSEMBLY AND CHECKOUT	37
Description of Gyro Assembly Steps	37
Use of a Tooling Gyro in Initial Checkout	39
Preparation of the Test Gyro	41
Mirror and Pickoff Alignment	42
PATTERN CALIBRATION AND READOUT ACCURACY	43
Calibration Data Samples	43
Considerations of Calibration Procedure	44
Calibration Data Acquisition Procedure	47
SDESG Data Processor Description	49
Pattern Mechanization Equation	52
Pattern Calibration Software	57
Readout Test Results	59
Appendix	
A FLEXOWRITER DATA FORMAT	A-1
B COMPUTER FORMAT OF CALIBRATION AND READOUT DATA	B-1

LIST OF ILLUSTRATIONS

Figure	Title	Page
1	Pattern Line Width and Spacing for Parameter Study	6
2	Comparison of Error Amplification for Two Readout Strategies and Two Pattern Line Types	10
3	Effect of Cosine Pattern Range on Uniformity of Mixed Mode Error	12
4	Laser, Aperture and Experimental Rotor	22
5	Laser Exposure Setup for Flat Samples	23
6	Laser Setup for Cosine Line Patterning	25
7	Microscope Setup for Rotor Pattern Examination	27
8	Rotor Patterning Machine	28
9	Portion of the Height Insensitive Trigger Circuit	35
10	Switching Curve for Original HIT Circuit	36
11	Switching Curve for Modified HIT Circuit	38
12	Strapdown Electrically Suspended Gyro	40
13	Laboratory Equipment	50

LIST OF TABLES

Table	Title	Page
1	Reflectivity of Candidate Coating Materials	16
2	Nozzle Dimensions	29
3	Nozzle/Grit Blast Ranking	31
4	Pattern Calibration and Readout	61

PERFORMANCE EVALUATION OF A STRAPDOWN ELECTRICALLY SUSPENDED GYRO FOR SPACE

By: Donald F. Elwell, John C. Wacker and James M. Miletich
Honeywell, Inc.

SUMMARY

This report describes the engineering development directed to improvement in strapdown Electrically Suspended Gyro (SD/ESG) readout accuracy. The results of this development effort were represented by new and modified parts which were assembled into a strapdown ESG which was evaluated in terms of its readout system accuracy.

The program performance goal was the demonstration of gyro readout to an accuracy of 15 arc-seconds or better. The results of calibrating over two sets of data were error amounts of 11.4 and 12.7 arc-seconds rms. The rms values of readout error were 12.7 and 13.8 arc-seconds for two sets of data not included in the calibration.

The techniques for rotor preparation which were investigated under this contract included the application of a thin metal coating to the rotor surface in addition to the use of bare, polished beryllium rotors. Patterning application means which were utilized included a laser for pattern exposure of a photoresist coating and a grit-blast patterning machine which applied the pattern directly onto the metal surface of the rotor.

Two rotors were completed ready for patterning; one was bare, polished beryllium and the other was beryllium coated with a thin layer of "Niculoy," a proprietary brand of non-magnetic nickel alloy plating material. The laser exposure of photoresist coating on the rotor resulted in a reasonably accurate mask being formed, but it was not as accurate as the pattern which could be applied directly to the rotor using the grit blast, patterning machine.

The two rotors which had been completed through the final fabrication step were patterned with the grit blast equipment. The nickel coated rotor was judged to be the most accurately patterned, so it was selected for assembly into the GG 432 A strapdown ESG which was furnished as Government equipment.

The gyro was assembled, pumped down to the required vacuum level of 5×10^{-7} Torr and pinched off. The gyro was then moved to the laboratory for alignment of the optical pickoffs and calibration of the applied pattern prior to the readout accuracy measurements.

PATTERN APPLICATION DEVELOPMENT

Pattern Analysis

Summary. - A study to determine the trade offs of a number of readout parameters was conducted in 1968 as part of a NASA-ERC sponsored program[1] on the SDESG. Included in the study were parameters such as pattern type, number of sets of pattern lines, number and arrangement of pickoffs, and readout strategy. Some specific recommendations were made on the value of each of these parameters:

- An orthogonal arrangement of three pickoffs provided more accuracy than a non-orthogonal arrangement of four pickoffs.
- Two sets of pattern lines provided slightly more accuracy than one set; however, since more lines would produce additional complexity to the pattern application process, the change to two sets was not specifically made.
- A readout strategy utilizing information from three pickoffs when available and two pickoffs when the third was beyond the pattern range was determined to provide best accuracy.

These conclusions were reached on the basis of minimizing error amplification of the type of errors characterized by pattern line edge uncertainty. This type of error was shown in the study to be a dominant factor in readout error.

Some attention was given to the trade-offs among three pattern types; great circle, cosine, and colatitude. They were examined in the context of several criteria-error amplification, ease of application, and computer mechanization requirements. The great circle pattern had the largest error amplification but was the easiest to apply. On the other hand, the cosine pattern had the smallest error amplification but was the most difficult to apply.

---

[1]"Research in Electrically Supported Vacuum Gyroscope - Volume IV - ESVG Readout Accuracy Improvement Research," November 1968, prepared under Contract NAS-12-542 by Honeywell, Inc.

- In the previous study, a normalization formula for the three-pickoffs was developed as part of the analysis, but it was not implemented in the computer program used in the strategy comparison study. For this study, the program was modified to implement this formula.

These refinements are described in some detail before the results are presented.

Pattern line spacing. - Some spacing is needed between pattern lines in order for the readout logic to discriminate between pattern lines. In addition, some allowance must be made for the fact that the lines have a discrete width. The pattern makeup, the width of each line, and the spacing between them for the purposes of the trade-off study is shown in Figure 1. The readout lines are the two narrow lines; the left edge of each (trailing edge) is the critical edge in the phase angle measurement. The pattern lines are symmetric in that they have equal and opposite slopes. The wide line leads one of the narrow lines; it enables the logic to discriminate between the pattern lines.

The critical spacing occurs at the extremities of the patterned region. The basic spacing parameter occurs between the logic line and the parallel pattern line, and is denoted by x in Figure 1. This is a linear parameter which is determined by the width of the pattern line, the space between the two adjacent line edges, and the slope of the pattern line at that point. A spacing equal to 2x is needed between the pattern lines at one extremity, and between the second pattern line and the logic line at the other extremity. Therefore, a spacing allotment of 5x (two times 2x plus x) is deducted from the spacing allowed from each pattern line equally.

For the purpose of this study, the assumed width of each pattern line was taken at 0.012 inch. The width of the logic line should be approximately double that, or 0.024 inch, and the minimum spacing between these two lines should be double the width of the logic line, or 0.048 inch, measured orthogonal to the line as shown in Figure 1. Consequently, x is determined by the equation

$$x = \frac{0.060}{\sin \delta} \text{ inch,}$$

where δ is the angle between the line at its extremity and the colatitude line. Since

$$\delta = \tan^{-1} \frac{d\theta}{d\Phi}$$

Appendix B

COMPUTER FORMAT OF CALIBRATION AND READOUT DATA

The computer program written for the purpose of calibrating the pattern mechanization polynomial coefficients has in its output format tables of calibration and readout errors. Two calibration tables are reproduced below; Table B-1 is the result of calibrating over readout data points separated by five-degree increments, and Table B-2 is based upon calibration over readout data points separated by one-, two- or five-degree increments. This is the same data from which the pattern calibration results were calculated. The column headings used in the tables are:

Colatitude - The angular measure between the No. 2 pickoff line of sight and the rotor spin axis.

Count Ratio - Ratio of the time interval between passage of the pattern lines to the time interval for one full revolution of the rotor.

Compensated Colatitude - Each data point, initially listed according to its count ratio in column two, has been adjusted according to the compensation curve which was computed upon the entire set of calibration data points.

Calibration Error - This is the error in degrees between the measured colatitude angle listed in column one and the compensated colatitude angle in column three.

INTRODUCTION

The program goal was to improve the readout accuracy of a strapdown ESG which utilizes a set of these electro-optical pickoffs viewing a line pattern applied to the surface of the gyro rotor.

The family of electrically suspended gyros has demonstrated high performance in the laboratory, aircraft navigation and shipboard navigation. The strapdown ESG has many desirable features when considering potential applications for attitude reference in space. The strapdown ESG has adequate or better drift performance than required for virtually all known and planned missions. The power requirements for the gyro are moderate, and its expected life in a space mission is measured in many thousands of hours. Up until the time of this AAFE contract, one performance factor lagged several mission requirements; this was the need for accurate readout. The goal established for this contract was the improvement of readout accuracy to 15 arc-seconds and the demonstration of the improved readout through the test of a modified strapdown ESG incorporating the new readout features.

TABLE B-2. PATTERN CALIBRATION - FIVE-, TWO- AND ONE-DEGREE INCREMENTS

Colatitude	Count Ratio	Compensated Colatitude	Calibration Error (degrees)
135,06151	,28499010	135,06138	-,00012
134,05692	,29407290	134,05960	,00268
133,05292	,30273260	133,04904	-,00387
132,04861	,31067010	132,04898	,00037
131,04431	,31866650	131,04355	-,00076
130,04001	,32611840	130,03800	-,00201
127,99412	,34032000	127,99648	,00236
125,99058	,35321980	125,99370	,00312
125,40906	,35682420	125,40796	-,00110
120,40644	,38505080	120,41082	,00438
115,40474	,40988390	115,39922	-,00552
105,40094	,45300800	105,40549	,00455
110,40316	,43227350	110,39960	-,00356
100,39915	,47272400	100,39662	-,00253
95,39275	,49178640	95,39247	-,00028
90,39493	,51056749	90,39641	,00157
85,42084	,52937029	85,42283	,00199
80,42230	,54875930	80,41896	-,00334
75,42368	,56897049	75,42882	,00514
70,42514	,59059639	70,42648	,00134
65,42645	,61422630	65,42312	-,00333
60,42770	,64073920	60,41899	-,00871
55,42891	,67131740	55,43468	,00577
54,02871	,68095300	54,02944	,00073
52,03191	,69559800	52,03658	,00477
50,08656	,71124110	50,08917	,00261
49,09008	,71991900	49,08604	-,00404
48,09360	,72903280	48,08987	-,00373
46,10195	,74905000	46,10293	,00098

The computation of the three direction cosines, which provide the measure of gyro spin axis attitude in the operational use of the gyro, is only slightly more complicated when obtained from a great circle pattern as compared to a cosine line pattern. The great circle line can be applied simply by rotating the rotor around a selected patterning axis without having to simultaneously translate the patterning tool as is required in patterning a cosine line on a spherical rotor. The great circle line patterned by means of the grit blast technique on its associated patterning machine can utilize a rectangular nozzle which was determined to have the minimum overspray error of all nozzle geometry tested. The cosine line pattern can only be applied with a circular nozzle because of the requirement posed by a continuously changing slope (direction) of the pattern; none of the circular nozzles tested were free of an overspray effect.

The great circle line was judged best of the candidate pattern lines in terms of least pattern line edge errors contributed by patterning machine positional error and by overspray effect. These factors were judged to outweigh the higher error magnification effect associated with the great circle pattern when compared with the cosine line pattern. On this basis, plus the supporting analysis and experimentation, a grit-blasted, great circle line pattern was selected for the rotors manufactured under the program.

Continued studies conducted. - The trade-off study on readout strategy in the previous program was conducted using the cosine pattern exclusively. It was determined in this study that it was beneficial to utilize the information from all three pickoffs, when it is available, to determine the spin vector direction rather than choose the two pickoffs which were most nearly centered in the patterned area. The benefit was great enough, from an overall accuracy standpoint, that it was helpful to increase the rotor pattern range (at a small sacrifice of accuracy on a per-pickoff basis) to increase the frequency of three-pickoff events relative to the two-pickoff events.

A similar strategy comparison was needed in our current program on the great circle pattern. Once this was completed, the optimum range and strategy for each pattern type could be compared in the final selection step.

Before the computer-aided strategy comparison was made, two refinements were made to the analysis:

- In the previous study, a fixed angular margin of two degrees was added to the nominal pattern range to allow for separation between pattern lines required by the readout logic. For this study, specific spacings and line widths were assumed.

TABLE B-3. READOUT ACCURACY RESULTS
BASED UPON PATTERN CALIBRATION
OVER FIVE-, TWO- AND ONE-DEGREE INCREMENTS

Colatitude	Count Ratio	Compensated Readout	Readout Error (degrees)
50.42992	.70836169	50.43402	.00410
56.02575	.66742899	56.02345	-.00230
60.01969	.64303460	60.01607	-.00362
89.97715	.51215959	89.97287	-.00428
121.98493	.37661530	121.98159	-.00334
130.41138	.32340730	130.40896	-.00243
135.41317	.28161500	135.41885	.00569

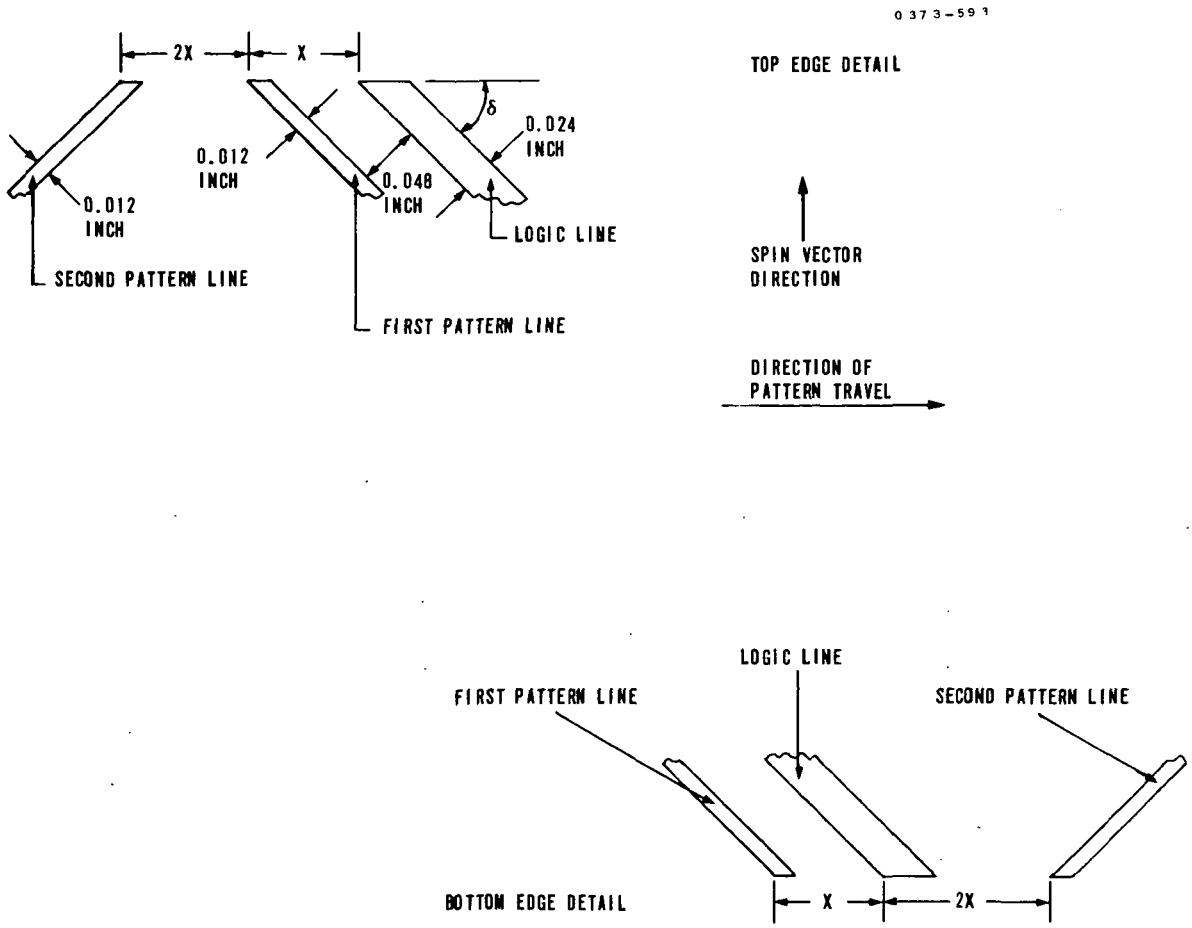


Figure 1. Pattern Line Width and Spacing for Parameter Study

then

$$\sin \delta = \frac{\frac{d\theta}{d\Phi}}{\sqrt{1 + \left(\frac{d\theta}{d\Phi}\right)^2}}$$

where θ denotes the colatitude variable and Φ denotes the longitude variable.

The angle represented by x is given by

$$\Phi_x = \frac{x}{r \sin \theta} = \frac{0.060 \sqrt{1 + \left(\frac{d\theta}{d\Phi}\right)^2}}{\sin \frac{d\theta}{d\Phi}}$$

since r = 1 inch for the SDESG rotor.

The specific pattern parameters are defined in terms of a point-to-point representation--one point being its intersection at the equator, and the other being the coordinate location of an extremity. Since the lines are symmetric about the equatorial intersect, line parameterization can be done by considering that half of the line is on the spin axis end of the rotor. The total spacing, when divided, requires that $1.25\ \Phi_x$ be deducted from the longitude range allotment for each half of each pattern line. If the equatorial intercept for one line occurs at $\Phi = O$, then the longitude coordinate at its extremity occurs at

$$\Phi_O = \frac{1}{n}\left(\frac{\pi}{2} - \frac{0.075 \sqrt{1 + \left(\frac{d\theta}{d\Phi}\right)^2_O}}{\sin \theta_O \left(\frac{d\theta}{d\Phi}\right)_O}\right)$$

where n is the number of sets of pattern lines placed on the rotor. (This parameter n is included in order to be consistent with the earlier study.) This equation is solved simultaneously with the equation of the line to determine the longitude coordinate Φ_O for a given θ_O which is specified by the pattern range under consideration.

Line edge error estimation. - The formulas for estimating the probable direction cosine error produced by line edge error were developed in detail in the earlier study and remain valid for the purpose of the extended study. Consequently, they will not be discussed in detail here. However, since the choice between a two-pickoff mode is an important part of the extension, these modes are briefly reviewed here.

The specification of the spin vector orientation is provided by measuring the direction cosines α, β, γ with respect to a stator fixed set of coordinates. The three pickoffs used in the SDESG are nominally orthogonal; hence, they form a convenient set of coordinates for direction cosine measurement. If errors $\Delta\alpha$, $\Delta\beta$, $\Delta\gamma$ occur in the direction cosine measurement, the spin vector description is in error by

$$\overrightarrow{\Delta S} = \Delta\alpha \hat{i} + \Delta\beta \hat{j} + \Delta\gamma \hat{k}$$

It is convenient to describe the error in terms of a scalar representation of ΔS; consequently, the square of ΔS is used for that purpose:

$$\Delta S^2 = \Delta\alpha^2 + \Delta\beta^2 + \Delta\gamma^2$$

The expected values of $\Delta\alpha$, $\Delta\beta$, $\Delta\gamma$ are zero, consequently, their variances are equal to the expected value of $\Delta\alpha^2$, $\Delta\beta^2$, and $\Delta\gamma^2$. Thus,

$$\delta^2(\overrightarrow{\Delta S}) = \delta^2(\Delta\alpha) + \delta^2(\Delta\beta) + \delta^2(\Delta\gamma)$$

When the two-pickoff mode is utilized, two direction cosines are provided by direct measurement. The magnitude of the third is calculated from the orthogonality identity

$$\alpha^2 + \beta^2 + \gamma^2 \equiv 1$$

and the sign is determined from past information or other suitable criteria. Errors in the measurement of the two cosines are propagated into the third through the identity. If it is assumed that α and β are measured with errors $\Delta\alpha$ and $\Delta\beta$, then it can be shown that

$$\delta^2(\overrightarrow{\Delta S}) = \frac{1}{1 - \alpha^2 - \beta^2} \left[(1 - \beta^2)\,\delta^2(\Delta\alpha) + (1 - \alpha^2)\,\delta^2(\Delta\beta) \right] \quad (2)$$

If the three pickoff mode is utilized, all three direction cosines are specified by direct measurement. If errors occur, ΔS^2 is given directly by (1) above. In this case, $\vec{S}$ may or may not be a unit vector. If it is not, it is produced by an error. In this case, the orthogonality identity may be used to make corrections and reduce the probability of error. If ordinary normalization is used, then the variance of $\overrightarrow{\Delta S}$ is

$$\delta^2(\overrightarrow{\Delta S}) = (1 - \alpha^2)\,\delta^2(\Delta\alpha) + (1 - \beta^2)\,\delta^2(\Delta\beta) + (1 - \gamma^2)\,\delta^2(\Delta\gamma) \quad (3)$$

Even when the pattern range is the minimum required to assure that two of the three pickoffs view the pattern at all times, there are frequent occasions when all three pickoffs will view the pattern. When this occurs, four choices are available for the readout cycle; three different combinations of two pickoffs, or all three pickoffs. The earlier study showed that, in general, the best choice from an overall accuracy standpoint is a three-pickoff mode which included spin vector normalization as a part of the direction cosine computation cycle. That this is the case can be deduced intuitively simply from the fact that more information is utilized for the readout cycle, hence, the probable error could be expected to be smaller.

The existing SDESG readout instrumentation utilizes two time interval measurement counters which provided the capability of phase angle measurement of the pulses from two pickoffs simultaneously. A simultaneous measurement of the three pickoffs was not possible, hence, two pickoffs have been utilized even when three pickoffs viewed the pattern. Under these circumstances, tha pair combination yielding the least probable error was utilized.

From Equation (2) it can be seen that the best combination is the pair that yields the largest value for the denominator term. The two pickoffs whose direction cosines are the smallest should then be used to yield the largest denominator; in other words the two pickoffs viewing regions nearest the rotor equator are likely to result in minimum two-pickoff mode error.

Results. - The results fo the extension to the earlier study are presented in the graph of Figure 2. The top edge of the pattern is given on the abscissa, the bottom edge is symmetrically located on the other side of the rotor equator. The results of two distinct strategies are shown for the great circle and for the cosine pattern:

- An exclusively two-pickoff mode strategy where the two pickoffs nearest the equator are used when a choice is available.

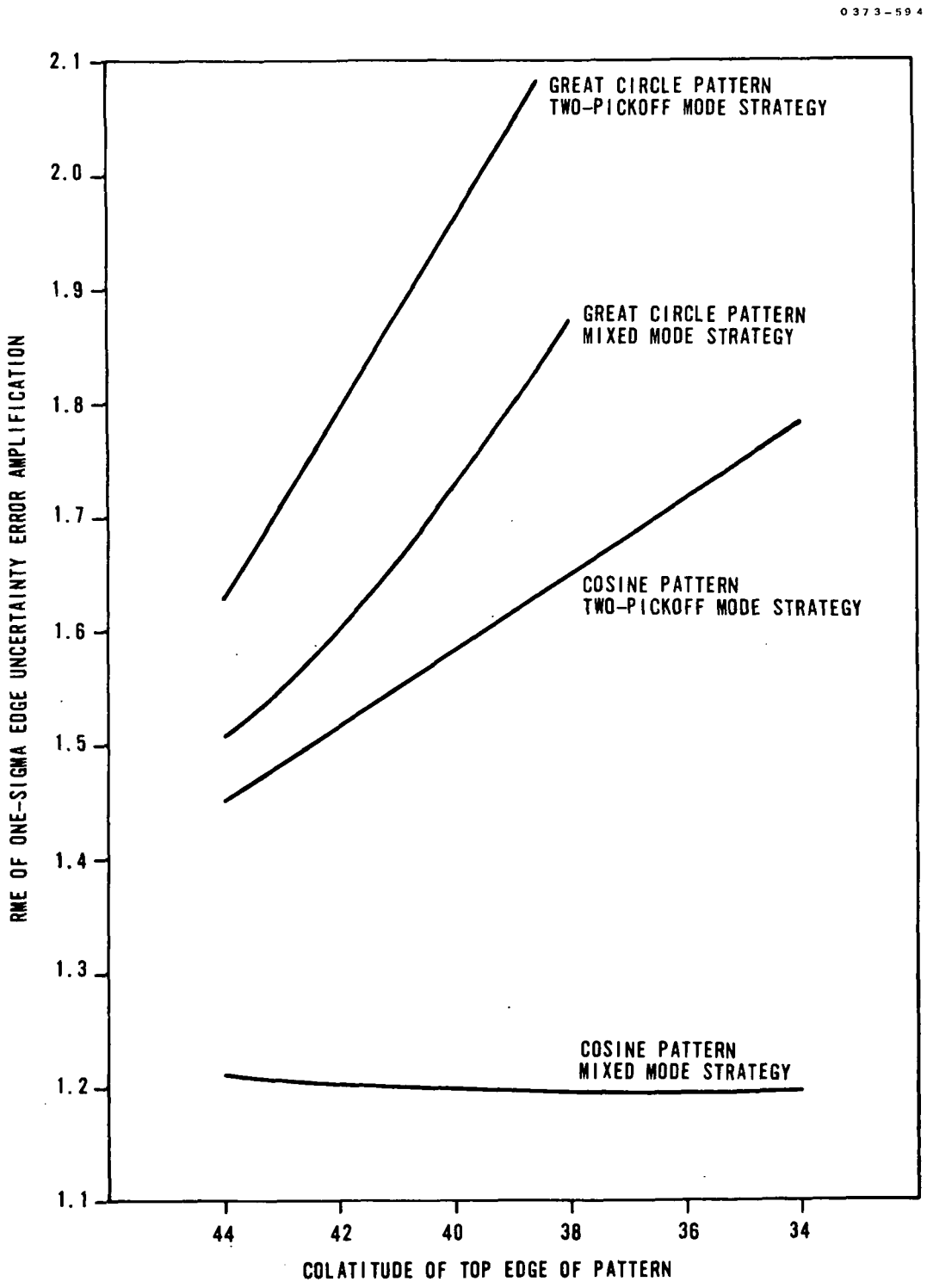


Figure 2. Comparison of Error Amplification for Two Readout Strategies And Two Pattern Line Types

- A mixed-mode strategy in which all three pickoffs are used when available and two pickoffs used when the third is not viewing a patterned region of the rotor. Normalization is assumed to be performed with the three pickoff mode.

The ordinate value denotes the RMS value of one sigma amplification of pattern line edge uncertainty [square roots of Equations (2) and (3)].

It can be seen that both strategies result in error curves that monotonically increase with pattern range in the case of the great circle pattern. The optimum range is approximately the minimum range needed for two-pickoff availability at all times.

The two-pickoff strategy for the cosine pattern is also monotonically increasing with pattern range; however, the mixed strategy curve is not. With the more realistic computation included for spacing margin and for normalized three-pickoff mode error included, a minimum in this curve occurs near the 37 degree pattern range point.

The curves of Figure 3 show how extending the range of the cosine pattern can be used to produce a more uniform amplification of error. The mixed mode strategy curve is repeated. Converging with the mixed mode strategy curve is the error amplification resulting from the use of all three pickoffs; convergence occurs because the mixed mode strategy employs the three-pickoff mode more frequently as the pattern range increases.

The other two curves are the minimum and maximum expected amplification of line edge error of the mixed-mode strategy. Both of them come from the two-pickoff mode: the minimum occurs when both pickoffs are viewing the rotor equator, and the maximum occurs when the field of view of the third pickoff lies just beyond the patterned region of the rotor. The maximum and minimum tend to converge as the pattern range is extended.

Consequently, the error amplification tends to become more uniform as the range of the cosine pattern is extended.

It was noted in this study that the three-pickoff mode with normalization using a cosine pattern yields an error amplification which is independent of spin vector orientation, but depends only of the pattern parameters. The error produced by edge uncertainty of a cosine line was derived in the

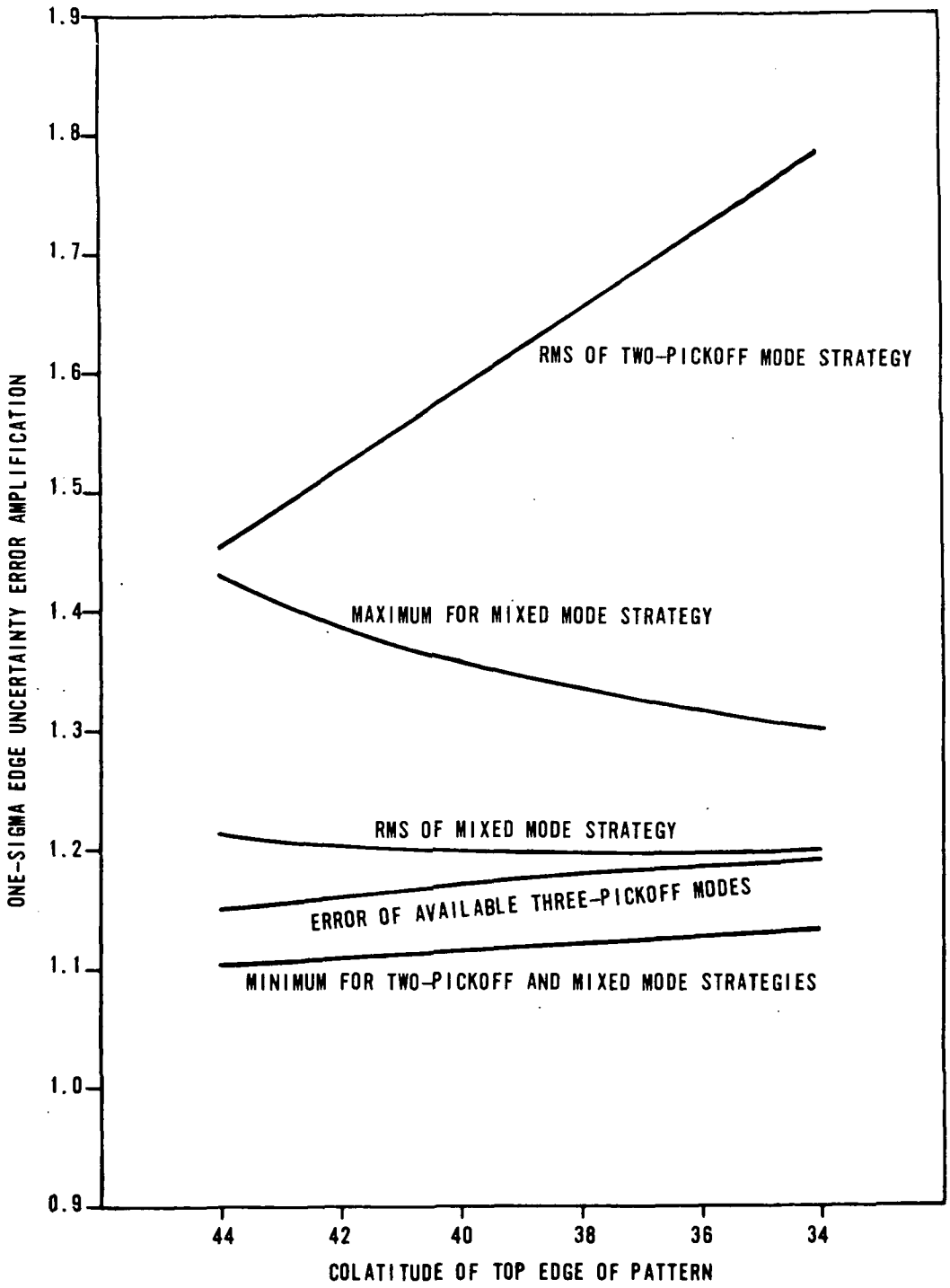


Figure 3. Effect of Cosine Pattern Range on Uniformity of Mixed Mode Error

earlier study; it is repeated here with the colatitude angle replaced by its cosine:

$$\delta(\Delta\alpha) = \frac{\epsilon}{r}\sqrt{\frac{2n\cos^2\theta_o}{\pi^2(1-\alpha^2)} + \frac{1}{2n}}$$

where ϵ is the linear line edge uncertainty.

Substituting this equation (and similar ones for $\alpha(\Delta\beta)$ and $\delta(\Delta\gamma)$ into Equation (3) and simplifying yields

$$\delta^2\overrightarrow{(\Delta S)} = \frac{\epsilon^2}{r^2}\left[\frac{6n\cos^2\theta_o}{\pi^2} + \frac{1}{n}\right]$$

As long as it is possible without sacrificing overall accuracy, an extension of the pattern range would be desirable to improve error uniformity. Figure 2 shows that this is possible when the cosine pattern is used. On the other hand, such an extension of the great circle pattern increases overall error; from this standpoint, the minimum range great circle pattern would be preferred.

The significant improvement that an optimized cosine pattern/mixed mode strategy offers over other strategies and the great circle pattern are attributed to pattern type:

- The smaller the slope of the pattern (intersecting angle with a latitude line), the smaller the edge error amplification. The cosine pattern slope is minimized in the equatorial regions, where the frequency of pickoff viewing is the highest. The slope of the great circle pattern, in contrast, is greatest at the equator.

- The great circle slope is a minimum at the extremities of the pattern range. For this reason, more linear distance is required for line spacing of great circle lines.

- Three-pickoff mode usage occurs at those occasions where the per-pickoff probable error, as a function of probable colatitude, is greatest for the cosine pattern; namely, when at least two pickoffs are viewing remote from the equator. This is in contrast to the great circle pattern; the peak error occurs at the equatorial region, a region at which a three-pickoff mode occurrance is less likely to occur and be of the greatest benefit.

With error amplification parameters having been delineated for the great circle and cosine patterns, the edge error requirements can now be specified for each to achieve the accuracy goals of this program. For a great circle pattern, the minimum range, with some margin to assure that at least two pickoffs view the pattern at all times, is selected; the pattern line is assumed to terminate at colatitude of 43 degrees; this results in an amplification factor (from Figure 2) of 1.55. Therefore, the edge resolution is given by

$$\epsilon = \frac{\delta\,\overrightarrow{(\Delta S)} \cdot r}{1.55}$$

where $\delta\,\overrightarrow{(\Delta S)}$ is set at 15 sec. This results in an edge resolution of 47 microinches.

For the cosine pattern, the optimum range of 37 degrees is selected; this results in an error amplification factor of 1.20. The edge resolution needed on the cosine pattern is given by

$$\epsilon = \frac{\delta\,\overrightarrow{(\Delta S)} \cdot r}{1.20}$$

or 60 microinches.

Rotor Surface Treatment

Preparation of the beryllium surface. - After grinding the hollow rotors to an oversize condition, preparation of the rotor surface and concurrent fine balancing is carried out. The rotors are lapped initially in cast iron laps, and these laps are supplied with successively decreasing grit sizes of aluminum oxide. Fine lapping of the rotor surface occurs with No. 10 (one micron) aluminum oxide mixed with water; the lap material for this operation is lucite. The result of the fine lapping operation is a matte finish on the rotor. Unbalance of the rotor is held to a limit of 0.2 dyne-centimeter; the unbalance is determined by immersing the rotor in a quiescent tank of pentane fluid and then timing its oscillatory period. The period of oscillation is then converted to rotor unbalance. Correction of excessive mass unbalance is done by preferential lapping force applied in such a manner that final requirements on rotor sphericity are also met.

The final surface treatment for the uncoated, bare beryllium rotor is a polish in a felt lap; cerium oxide is used as the polishing agent. The beryllium surface of the rotor is polished until it meets a requirement of forty percent reflectivity (minimum) as measured with an optical pickoff and shutter device adopted from the gyro pickoff itself. The measuring device is calibrated with a polished silver reference surface which results in a reflectivity reading of 93 percent. The balanced, polished rotor is then ready for patterning.

Comparison of selected coating materials. - One of the major tasks of the program was to determine the feasibility of applying a surface coat to the beryllium rotor to improve readout characteristics. Such improvements were expected to consist of:

- Higher reflectivity contrast between unpatterned and patterned areas.
- Resistance to blemishing caused by discharges between the rotor and electrodes.

A higher contrast would raise the optical signal received by the pickoff while the blemish resistance would reduce an important noise factor in that signal. Adherence of a candidate coating material to the rotor was a key factor to be determined because either "bubbling" of the material or particle breakaway would be damaging to the gyro. From the standpoint of gyro drift performance, the coating could not exhibit magnetic properties.

The coating finally selected is a proprietary alloy named Niculoy 22 by the supplier, Shipley Corporation. The alloy consists of phosphorus, copper and nickel with the nickel being the major constituent.

Selection and testing candidate materials. - The selection of candidate materials was based upon known general reflectivity and expected blemish resistance from discharges. Materials which evaporated at high temperatures were considered prime candidates -- namely, nickel, niobium, chromium, and tungsten. Of these materials, nickel is the only one whose thermal expansion coefficient comes close to matching that of beryllium; consequently, it was the only one that could be tested as a plating material. All of these materials were candidates as sputtered coats which would be applied in a much thinner coating than that applied by plating.

Reflectivity tests. - Reflectivity tests were conducted on glass slides on which the candidate materials were sputtered. This served to rank the materials in a relative sense. Nickel and chromium ranked higher in reflectivity than niobium and tungsten.

More important, however, were reflectivity tests conducted with these materials sputtered onto polished beryllium test pieces. Because sputtered coats are thin, the surface finish of the coats is determined to some extent by the surface finish of the substrate; consequently, the glass slide measurements alone could not be construed to represent the reflectivity of sputtered coats on beryllium. A comparison of reflectivity measurements made on beryllium pieces sputtered with the candidate materials is given in Table 1.

TABLE 1. REFLECTIVITY OF CANDIDATE COATING MATERIALS

Candidate Material	Reflectivity[1]
Niculoy(TM)	62 percent
Nickel	58 percent
Chromium	57 percent
Niobium	54 percent

(1) The reflectivity readings are related to a calibration level of 93 percent light reflection from a polished silver sample.

Tensile tests. - Tensile strength tests were conducted on niobium sputtered test pieces with satisfactory results. These test pieces were then lapped down and plated with electroless nickel. The tensile test on this coat was not satisfactory, and, in fact, did not measure up to a similar nickel-plated beryllium strength test conducted for another program. Subsequent examination of the substrates indicated that the previous niobium coating was not completely removed. It was concluded that the presence of niobium prevented the bonding of nickel to beryllium to the strength indicated by the other test.

Shear tests. - Shear strength tests were also conducted on niobium sputtered and nickel plated beryllium pieces. Satisfactory results were obtained with both coats.

Magnetic susceptibility tests. - The glass slide samples were utilized in tests to qualitatively determine the presence of ferromagnetism or paramagnetism in their sputtered coats. Only the nickel sputtered coat showed some ferromagnetic characteristics. The quantity of sputtered material was too small to provide measurements that would yield any more than a qualitative indication of their properties.

The search for an optimum coating material was then directed toward a nickel alloy that could be electroplated; the alloy utilized in electroless-nickel plating was claimed to be free of residual magnetic properties. The plating procedure for electroless nickel is one of critical importance in attaining the desired nonmagnetic properties in the resultant coating. Tested along with the electroless-nickel plating was the "Niculoy" alloy which is nonmagnetic without critical dependence on the plating material. The reflectivity of the "Niculoy" was measured to be higher than the electroless-nickel samples tested concurrently.

Preparation of the "Niculoy" coating. - Two different approaches were attempted in coating candidate rotors with Niculoy. One approach consisted of activating the beryllium surface and plating Niculoy directly to the beryllium. This approach was not acceptable because the resultant surface was pitted in a few spots where the Niculoy failed to adhere to the beryllium. Examination of these pitted parts led to the suggestion of the second process which was tried experimentally and then utilized for the final rotor preparation.

The second process involves a cleaning similar to that used in the initial processing attempts, but then it switches to a very thin coat of zinc followed by a very thin coat of copper before the Niculoy is plated onto

the sphere. This technique provided a continuous, adhering coating over the beryllium, and the Niculoy plated well to the copper strike coat. The Niculoy plating process is outlined as follows:

a. Clean the rotor with acetone followed by immersion in potassium hydroxide electrocleaner.

b. Pickle the rotor in a combined solution of nitric and hydroflouric acid.

c. Rinse with de-ionized water.

d. Dip the rotor in a zinc immersion solution for a very thin coating.

e. Rinse with de-ionized water.

f. Copper strike plate the rotor for a second thin coat over the initial zinc layer.

g. Rinse with de-ionized water.

h. Plate with Niculoy to a thickness of 1.5 mils with continuous agitation of the solution to break up attached bubbles which could otherwise cause pitting of the surface.

i. Rinse with de-ionized water and bake as a final drying step.

This total process takes approximately eight hours to complete. At this point the rotor is ready for lapping and polishing which will bring the rotor back to its prescribed diameter with a final Niculoy coating thickness of 0.5 mil.

Laser Photoresist Method

A major area of the pattern application study was a feasibility study for laying out a cosine pattern on the rotor using a laser beam to expose a photoresist. If this study proved the feasibility of the method, a relatively simple mechanical setup could be used to accurately define the cosine line. The experiments conducted in this program established feasibility of the concept. It was determined, however, that to obtain the accuracy goals of this program, some refinement in the procedures relating to the usage of the photoresist in this technique is necessary. Program schedule requirements and resource budgeting did not permit development of these refinements to the point that the technique could be utilized for patterning a rotor for tests.

Concept. - The concept of using a laser beam to expose a photoresist for defining a pattern line developed from a method by which a cosine pattern line may be mechanized onto the rotor. This mechanization features a reference point which moves parallel to the rotor spin axis; at the same time, the rotation angle about the spin axis is changing. The ratio of the rate of translation of the reference point to the rotation rate is controlled to be a constant. A line (hereafter called the transfer line) is projected from the reference point which orthogonally intersects the spin axis. The locus of points that this transfer line describes on the rotor surface is a cosine pattern line.

It is relatively simple to mechanize the rotation of a rotor and the movement of a reference point parallel to the rotation axis. It would not be difficult to arrange a system so that the ratio of the rates may be changed to a different constant, so that the slope of the pattern line may be altered if necessary. The difficult aspect of the mechanization is to accurately transfer the reference point to the surface along the transfer line. This transfer must be accomplished in such a manner that the accuracy is not degraded by the variation in distance from the reference point to the rotor surface nor by the changing angle of incidence between the transfer line and the tangent plane at the intersection with the rotor surface. The use of a collimated beam of light appears to be a promising means to accomplish this transfer. In order to inscribe the surface with the beam, a film of photoresist would be placed on the rotor. Portions of this film would be exposed using the setup needed to describe the cosine line. The photoresist would then be developed; either the exposed or unexposed portion (depending on the type of photoresist used) would be removed from the surface. The boundary between covered and exposed portions of the rotor surface would then be the pattern line; subsequent processes (such as an etch of the exposed surface) would permanently inscribe the line on the surface. The final step would then be the removal of the rest of the photoresist from the surface.

Earlier pattern line application development programs featured experiments with photoresist techniques for applying a pattern mask. An ordinary light source was used for exposing the resist; it was determined that the source was the main limiting factor in utilizing the technique. There was insufficient resolution of the beam edge to provide the line edge resolution sought in that program. These findings suggested that a laser beam might be a better light source because a high intensity beam can be obtained with a relatively low divergence.

Laser and photoresist characteristics. - The choice of a laser was narrowed considerably by the need for a beam wavelength which was in the photoresist sensitive range. Photoresists are generally sensitive to blue near ultraviolet wavelengths while most lasers are in the red and infrared ranges. The laser selected for use in the experiments was a Spectra-Physics Model 185 helium-cadmium laser (single-isotope option 03). This laser is capable of producing 50 milliwatts at 441.6 nm, or 15 milliwatts at 325.0 nm. The shorter wavelength was chosen for the experiments because of the greater beam resolution capability at this wavelength. The difference in output power was not considered significant; this factor could be compensated by adjusting the rate at which the beam passes across the photoresist.

Only positive photoresists (where the exposed portions are removed during development) were considered as suitable for the experiments because:

- Those areas to be exposed to the light correspond to the areas of the rotor surface intended to be dark or diffuse after pattern application is complete.

- The exposed areas were expected to comprise a small portion of the total area to be covered with photoresist.

Exposing the areas to be made diffuse would cause no alteration of the rotor fabrication process before patterning, where the entire surface is brought to a bright finish. The patterning process renders selected areas (pattern lines) diffuse or dark; this constitutes a relatively small area to be exposed. The amount of photoresist to be removed during development (after exposure) is a minimum, which from a photoresist development standpoint is an apparent optimum situation.

The photoresists selected for the experiments were Shipley AZ111 and AZ1350. The AZ1350 has higher resolution capability but is not as durable as AZ111. If the AZ111 was determined to have a resolution compatible with our accuracy goal, then its greater durability (resistance to an etch solution) would make it a preferred choice for the pattern application process.

The energy needed from the beam to expose the photoresist depends on the chemical makeup of the photoresist and on the thickness of the coat on the sample. To obtain the general magnitude of edge resolution sought by this program, a relatively thin coat of photoresist is needed. Careful control must also be exercised on the uniformity of the coat when the photoresist is placed on the sample.

Another important factor affecting edge resolution is the profile of the beam intensity used to expose the photoresist. As emitted from the tube, the profile of a laser beam is a Gaussian curve about the center. Such a beam is not expected to provide the desired edge resolution. Greater resolution is possible by focusing the beam; an enhanced resolution is, in principle, available at or near the focal point of the beam. Another way to improve the edge resolution is to use an aperture to allow only the central portion of the beam to strike the photoresist. The effectiveness of this method of improvement is limited, however, by the diffraction which occurs around the edge of the aperture. The aperture is set up between the laser and the test rotor in Figure 4.

Experiment description. - All of the feasibility experiments were conducted with the sample pieces mounted on a milling machine table which could be moved horizontally at a constant rate. The laser was placed in front of the table and oriented so that its beam was horizontal and perpendicular to the direction of table travel. Fixtures were built so that flat or spherical sample pieces could be mounted on the table. Another fixture permitted the placement of a lens and/or aperture plate in the path of the laser beam. Exposure of the resist took place by positioning the piece at the proper height, then turning on the table drive to pass the sample across the beam.

The first set of experiments were conducted using flat steel samples. The purpose of these experiments was to determine the effectiveness of the beam to expose the resist, and to determine whether a sharper line edge might accrue by focusing the beam and/or passing the beam through a small aperture. The experimental setup (Figure 5) included micrometer positioning capability to permit precise vertical indexing between passes of a multiple-pass run; such a procedure would be used to expose an area several times the width of the beam diameter. The important conclusions from these experiments were:

- The beam intensity was adequate to fully expose the photoresist, with or without a lens.
- The use of a lens provided no significant improvement. Beam attenuation by absorption and scattering more than compensated for any potential improvement accrued by focusing the beam.
- Use of an aperture was effective in producing a sharp edge on the photoresist.

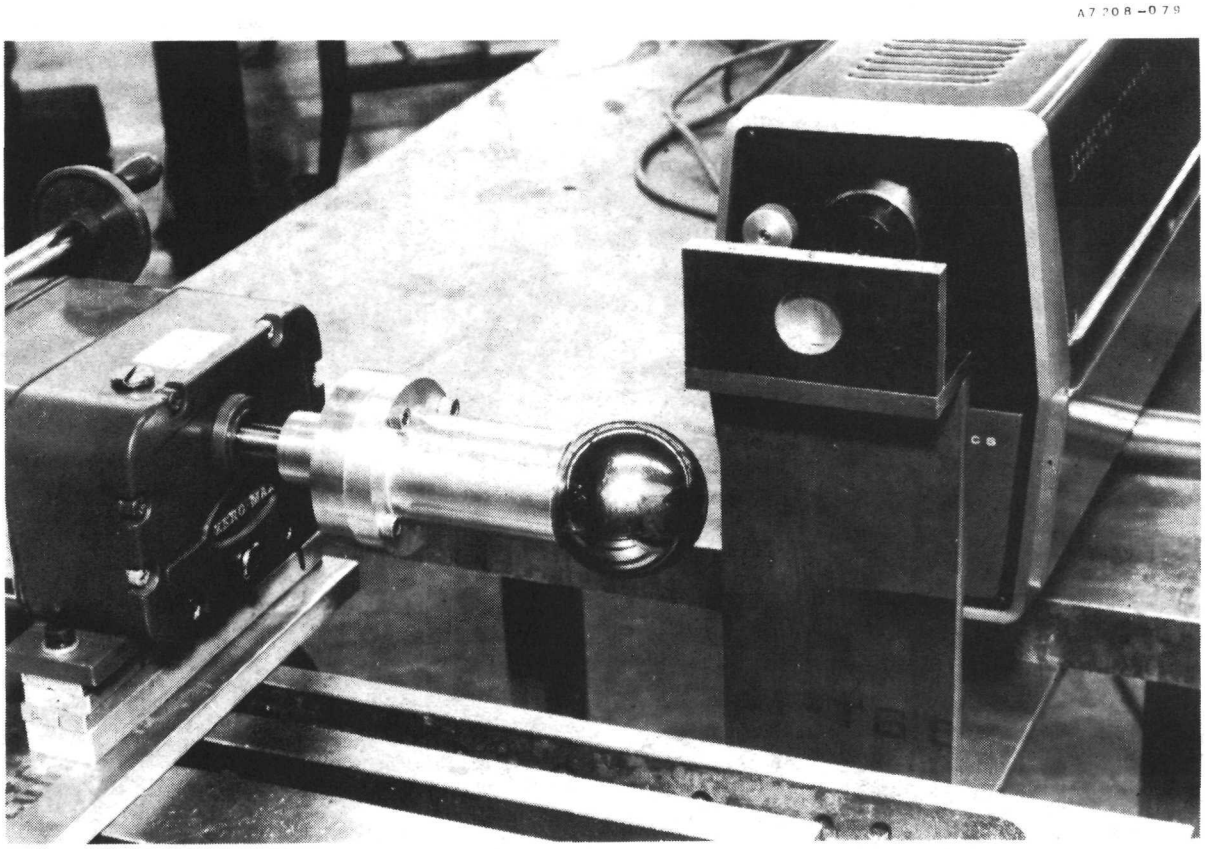


Figure 4. Laser, Aperture and Experimental Rotor

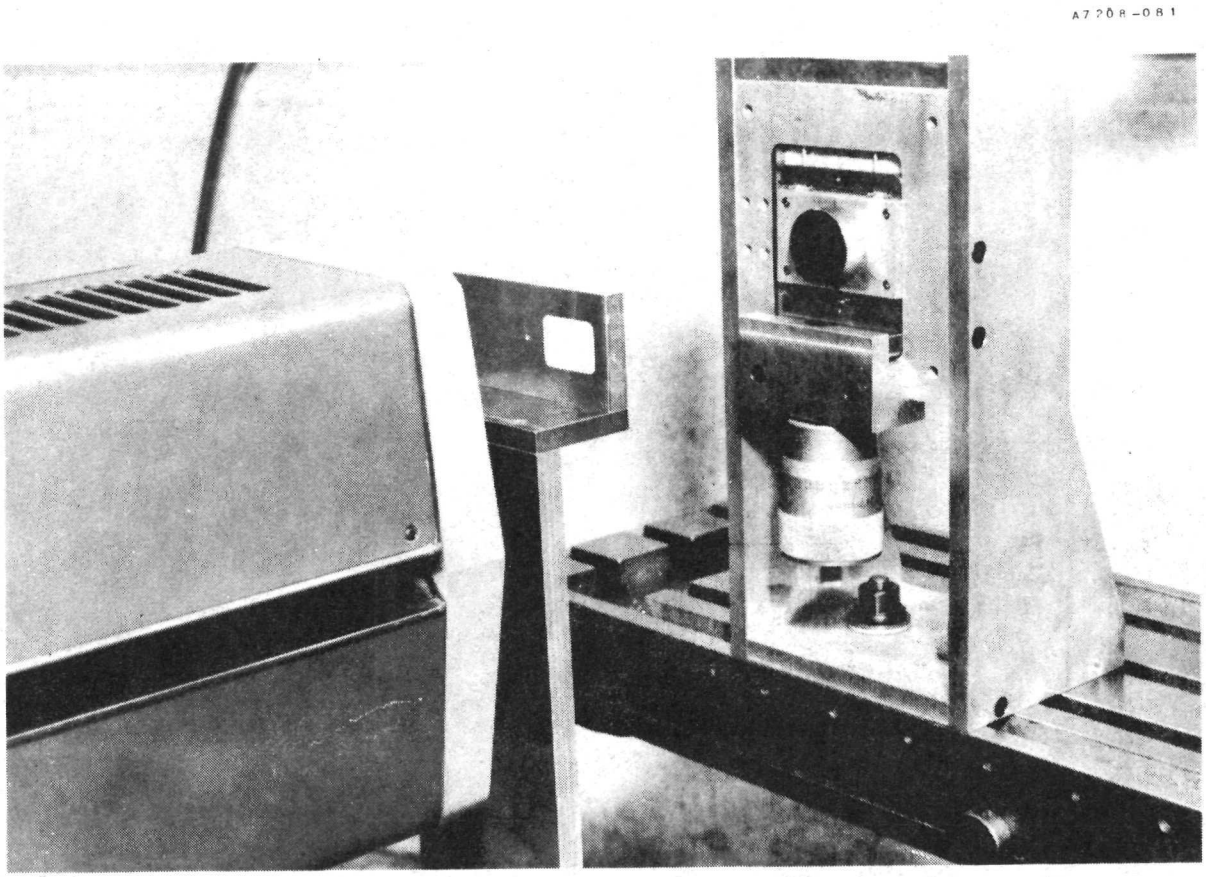


Figure 5. Laser Exposure Setup for Flat Samples

With the use of an aperture, the assumed plan of multiple passes across a small beam, and indexing the piece by the beam width between passes, was changed to a single pass with the beam aperture set to the desired width of the pattern line. Such a change would serve to simplify the procedural controls needed to expose the pattern line areas on the product rotor.

Subsequent experiments were conducted on spherical samples using the apertured beam. The purpose of these tests was to determine the effect of a changing beam length and angle of incidence on the location and resolution of the line edge. The effect of these changes is determined largely by the beam characteristics. If the beam is converging or diverging, the width of exposure would change with distance. If the beam is collimated, no significant changes would be observed.

A change of the angle of incidence would change the area of surface exposure. As this angle increases, a greater area is exposed. The beam intensity per unit of surface area is reduced; this can result in a narrower line at large angles of incidence. The severity of this effect is determined by the beam intensity profile; if it is substantially above the exposure threshold for the sample travel rate at zero angle of incidence across the entire apertured beam, the narrowing would be noticed only at the extreme angles of incidence. If on the other hand, there is significant variation at slightly above the threshold, the narrowing would be noticeable over the exposed region.

A setup for exposing a cosine pattern line on a spherical sample is shown in Figure 6. The sample is glued to the mandrel and mounted on the motor and gear reducer assembly. The base is mounted on the milling table. The height is adjusted so that the axis of rotation is at the top or bottom edge of the laser beam. As the motor rotates the sphere, the milling table moves the motor assembly so that the sphere passes across the laser beam.

To accurately evaluate the changes occurring in the exposed area as a result of beam distance and angle of incidence variations, it was desirable to place a redundant form of the cosine line on the sample. This would consist of a strip parallel to the equatorial plane of the sample, with the means of exposure designed to simulate the changing beam length and angle of incidence. This was accomplished in the experiments on the spherical samples by mounting the sphere and mandrel onto an adapter plate and mounting the plate onto the milling table with the axis of the mandrel in a vertical orientation. The sample is exposed by passing the sphere through the beam with the table drive mechanism.

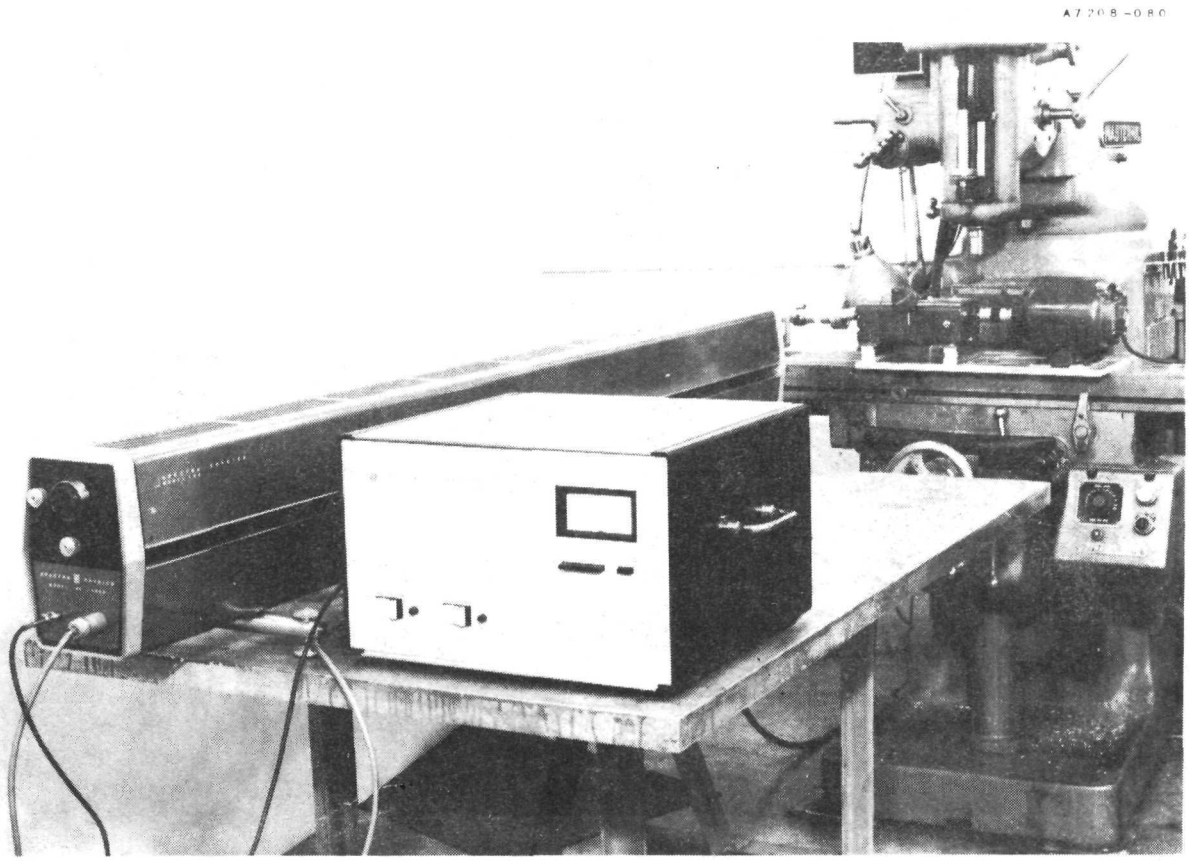


Figure 6. Laser Setup for Cosine Line Patterning

Test results. - Three spheres were mounted on mandrels and coated with photoresist. One was dipped in a solution of two parts AZ111 to one part of photoresist thinner. Another was coated with AZ1350 (undiluted) and the third was dipped in a mixture of one part AZ1350 to one part thinner. The spheres were withdrawn from the photoresist at the rate of 2 inches per minute and baked in an oven at 150°F for twenty minutes.

After exposure and development, the spheres were baked again at 150°F for twenty minutes. The test pieces were then mounted on the rotor patterning jig (Figure 7) for examination with the microscope. The unexposed and exposed areas were separated by a partially exposed area in which the thickness of the resist was tapered. The angle intercepted by the tapered region was 2 minutes of arc on the rotor coated with thinned AZ1350. The edge of the fully exposed area had a peak-to-peak uncertainty of approximately 30 seconds.

The line narrowing that could result from varying beam lengths and angles of incidence was not evident except at the extreme areas.

Patterning By Surface Abrasion

Description of the patterning machine. - The patterning jig (Figure 8) is used to compare various patterning techniques and to apply final patterns to rotors. The jig design incorporates a hydrostatic spindle whose runout is approximately 5 millionths total indicator reading (TIR) and which is driven by a servo motor with associated electronics. The speed of the servo motor can be varied continuously between 0.3 rpm and 5 rpm in either direction. An angle measuring device, "Unisec", is connected to the drive shaft between the drive motor and hydrostatic spindle. The "Unisec" permits the measurement of angular rotations of the spindle within 3 arc-seconds. The rotor to be patterned is mounted on the hydrostatic spindle above the left table. The left table is connected to the right table by a precision linkage so the movement of one table will be duplicated by the other table. A second "Unisec" is mounted on the right table so that rotation of either table can be measured within 3 arc-seconds. An air gage is used in aligning the rotor so that rotor runout will be less than 50 millionths.

A microscope is mounted on the left table for precision alignment of the spin axis of the rotor with the hydrostatic spindle axis of rotation and for the various angular measurements required in application of a great circle pattern. The air abrasive unit supplies the stream of gas propelled grit particles which "blast" the desired line on the rotor.

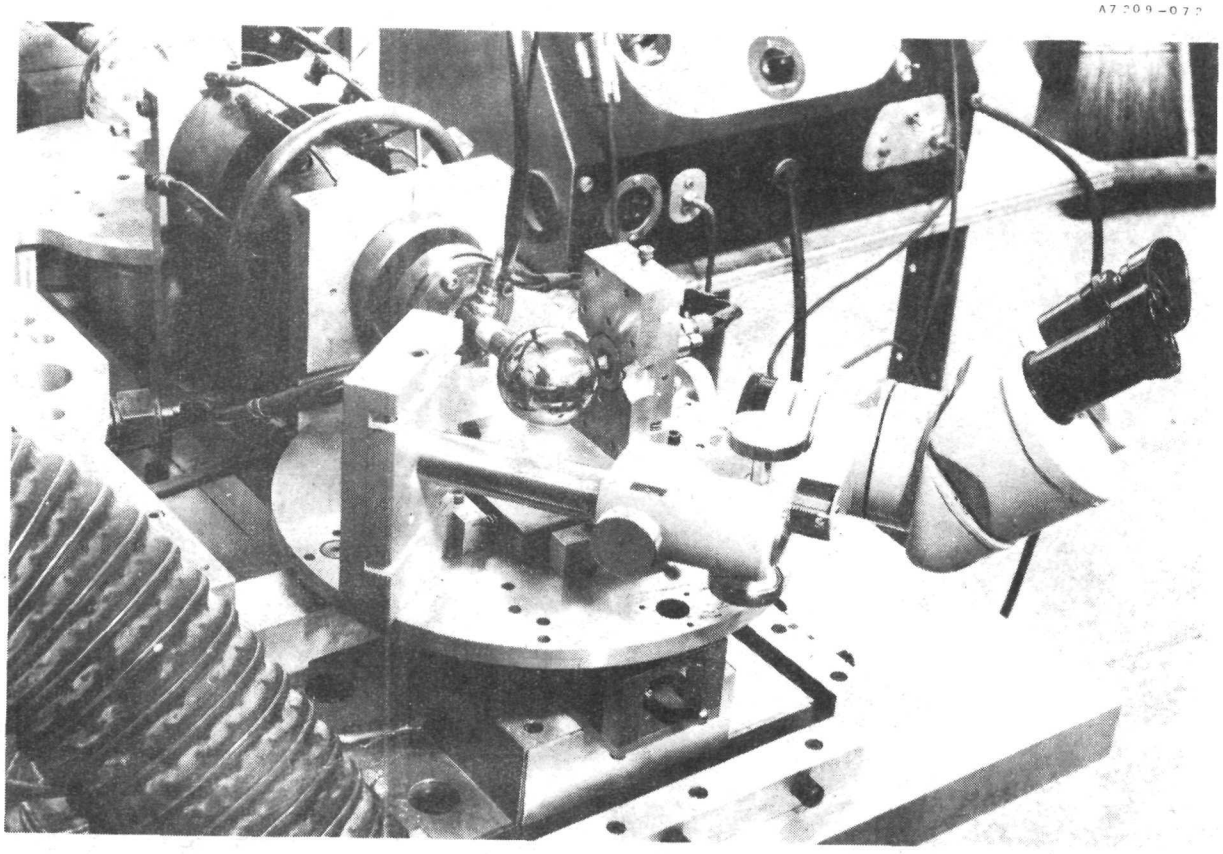


Figure 7. Microscope Setup for Rotor Pattern Examination

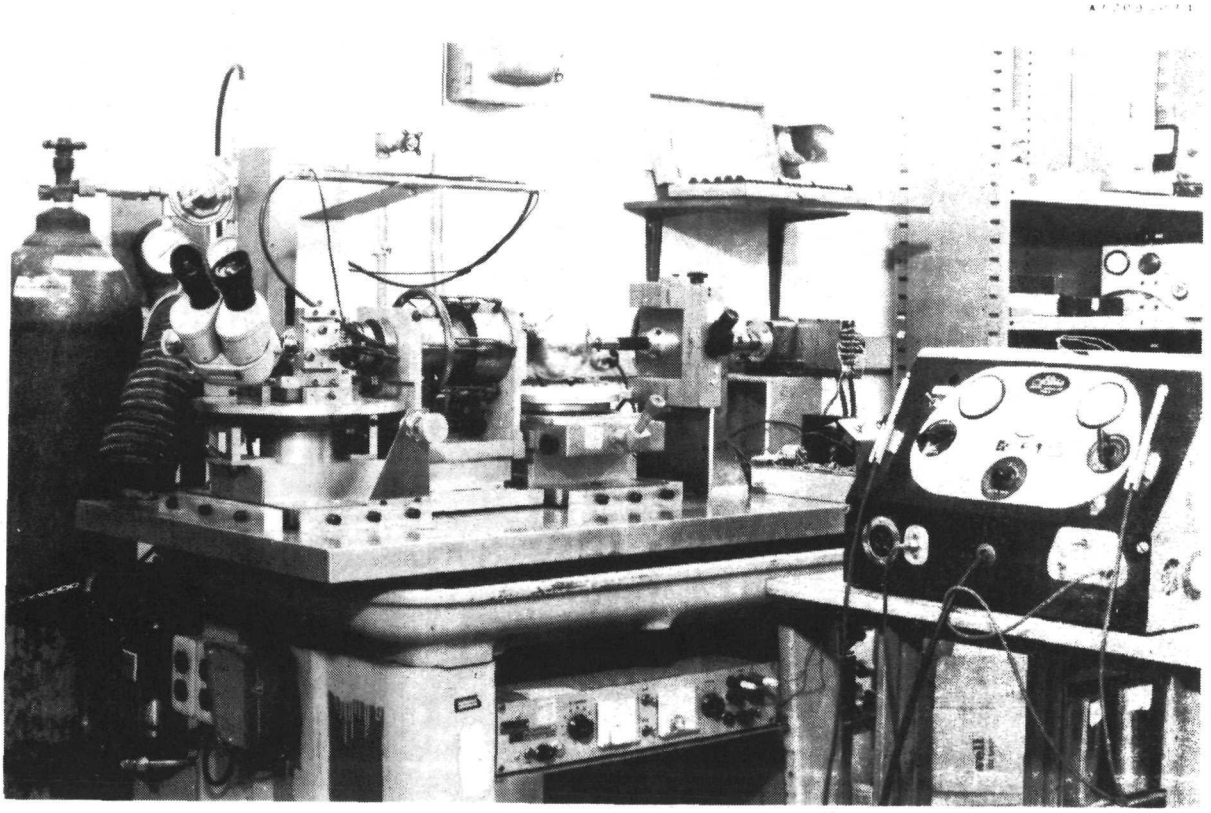


Figure 8. Rotor Patterning Machine

Experiments with patterning nozzle geometry. - Experiments in patterning with an air abrasive unit were conducted with various size nozzles of different geometry. All experiments were conducted utilizing either a polished beryllium rotor or a polished nickel-plated beryllium rotor. A table of the nozzles used is given in Table 2.

TABLE 2. - NOZZLE DIMENSIONS

Circular	Square	Rectangular
0.007 dia	0.026 sq	0.003 x 0.020
0.026 dia		0.003 x 0.060
		0.006 x 0.020
		0.006 x 0.075
		0.010 x 0.030

There are four major areas of interest in examining the quality of the various lines produced with the different nozzles. They are line darkness, line resolution, line overspray and surface disturbance.

To help eliminate overspray, the rotors are coated with several layers of lacquer layout dye which serves as an overspray mask. The lacquer serves a two-fold purpose in minimizing rotor patterning from those particles whose paths take them outside the projected inner wall boundaries of the nozzle and from those few particles which bounce back from the rotor line surface, strike the front surface of the nozzle wall, and then rebound toward the rotor again. Overspray is minimized by positioning the face of the nozzle within 0.003 inch of the rotor.

Lines made utilizing the 0.026 diameter circular and 0.026 square nozzle had acceptable line darkness and line resolution but had serious overspray. The cause of the overspray problem was judged to be from particles making secondary impact upon the rotor after "bouncing back" to hit the large front wall surface of these nozzles. The nozzle ends were tapered to minimize the front wall surface area in order to reduce overspray. Tapering did reduce the overspray but not to an acceptable level.

Lines made with the 0.003 x 0.060 and 0.006 x 0.075 nozzles exhibited good line darkness, line resolution and minimum overspray. The narrow rectangular geometry of these nozzles apparently eliminates the overspray problem completely. The 0.010 x 0.030 nozzle exhibited good line darkness and line resolution but had a small amount of overspray. Although the amount of overspray was greater than with the 0.003 x 0.060

or 0.006 x 0.075 nozzles, it was considerably better than the 0.026 diameter circular and 0.026 square nozzle. With an extra heavy coat of layout dye, it was possible to reduce the overspray to a minimum amount.

Lines made with the two rectangular nozzles (0.003 x 0.020 and 0.006 x 0.020) and the 0.007 diameter circular nozzle also exhibited good line darkness, line resolution and minimum overspray. A major difficulty with these nozzles was in applying a continuous line. The grit did not flow smoothly through the nozzle but was sporadic. The reason for the inconsistency with these orifice nozzles is believed due mainly to the "packing" tendency of the 10 micron grit. A larger grit, 27 micron, was used in an attempt to eliminate the sporadic grit flow. With the 27 micron grit, smooth grit flow was obtained but line resolution was not as good as obtained with 10 micron grit. If a line is to be applied with these nozzles, the 27 micron grit is required to insure the application of a uniform, continuous pattern line.

Several other variables, besides nozzle geometry and size, which affect line quality are propellant gas pressure, grit size, and quantity of grit flowing in the propellant gas stream.

The pressure of the dry nitrogen gas propellant is adjustable continuously between 25 psi and 80 psi. At high pressures, 70 to 80 psi, the pattern lines were lighter than those obtained with lower gas pressures. Also at lower pressures, overspray was decreased.

A comparison between lines applied with 10 micron and 27 micron grit showed that for all cases the 10 micron grit produced lines with better resolution and less surface disturbance.

The quantity of grit flowing in the propellant gas stream is controlled by means of a "shaker". Increasing the "shaker" voltage increases the quantity of grit particles in the gas stream. At low voltage settings, the shaker does not supply enough grit particles to produce a line of required darkness. For all cases, best line quality was obtained with the "shaker" on maximum.

The "best" line is obtained from either a 0.003 x 0.060 or 0.006 x 0.075 rectangular nozzle using 10 micron grit at a gas pressure of 30 psi and "shaker" voltage on maximum. A line would typically have a 12:1 reflectivity ratio, 90 microinches peak-to-peak line resolution, negligible overspray and 10-15 microinches surface disturbances. Table 3 ranks the nozzles according to the quality of line they produce. In selecting a nozzle for applying the pattern line, the main requirement is line resolution,

TABLE 3. - NOZZLE/GRIT BLAST RANKING

Rank	Nozzle	Grit Size	Gas Pressure	Shaker Volt
Best	0.003 x 0.060	10 micron	30 psi	Maximum
Best	0.006 x 0.075	10 micron	30 psi	Maximum
Good	0.010 x 0.030	10 micron	30 psi	Maximum
Good	0.003 x 0.020	27 micron	30 psi	Maximum
Good	0.006 x 0.020	27 micron	30 psi	Maximum
Good	0.007 dia cir	27 micron	30 psi	Maximum
Bad	0.026 dia cir	10 micron	30 psi	Maximum
Bad	0.026 sq	10 micron	30 psi	Maximum

since it has the greatest effect on readout accuracy. The 0.003 x 0.060 and 0.006 x 0.075 nozzles produced the best line resolution and also excelled in the other areas of interest. The 0.003 x 0.060 nozzle was selected for applying the pattern line.

The requirements for the logic line are not as strict since the logic does not furnish any data pulses. The 0.010 x 0.030 nozzle was selected for applying the logic line since a satisfactory line could be obtained using 10 micron grit.

The only noticeable difference between lines applied to beryllium rotors and a nickel-plated beryllium rotor was that the lines on the nickel-plated rotor were darker (less reflective).

The final variable which was found to have an effect on the pattern line application was the rate of rotation of the rotor while being grit blasted. A rate of 0.5 to 0.7 rpm was found to give the best results for all cases.

Description of selected pattern. - The pattern and application process selected for use in preparing the strapdown ESG for test are described as follows.

Pattern. - The pattern consists of a great circle inclined at an angle of 56 degrees at the equator of the rotor. The pattern line is terminated in both hemispheres of the rotor at a latitude of 47 degrees; this effectively separates the great circle into two line segments. On one side of the rotor, the line segment is paralleled with a logic line which precedes the pattern line according to the selected spin direction of the rotor. The two pattern line segments are 0.060 ≠ 0.004 wide. The logic line is

0.030 ≠ 0.004 wide, and it is separated by 0.060 from the pattern line. The goal established for pattern line uncertainty, measured at the trailing edge, is 80 microinches, peak-to-peak.

Pattern application. - The pattern application technique used on both the shiny beryllium rotor and the beryllium rotor is one of grit blasting the pattern and logic lines. The technique is outlined along with pertinent observations on each of the steps:

a. Rotor Preparation. The rotor spin axis is located and marked by running and stabilizing the rotor on an air bearing pad.

b. Mounting and Alignment of the Rotor on the Pattern Machine. Using a microscope with a cross-hair reference eyepiece, the rotor is positioned in the vacuum chuck of the patterning machine so the plane of the great circle pattern is perpendicular to the rotational axis of the mandrel.

c. Application of Layout Dye Mask. Layout dye is applied to the rotor in a uniform band of about one-half inch width centered about the intended track of the pattern line.

d. Termination of Lines in the Pole Regions. The pattern and logic lines are not applied in the high latitudes where the decreasing slope of the pattern degrades the potential readout accuracy. Metal-backed tape is applied to the rotor to stop the patterning grit from contacting the rotor beyond the selected pattern range.

e. Preparation of the Grit Blasting Machine. The machine is loaded with 10 micron aluminum oxide grit which is continuously heated to assure dryness. The gas supply of dry nitrogen is set up at 30 psi.

f. Alignment of Grit Blast Nozzle. The 0.003 x 0.060 nozzle is positioned with a 0.003 inch gap to the rotor in preparation for applying the pattern line; the same gap is used in setting up the 0.010 x 0.030 nozzle in applying the logic line. The machine-mounted nicroscope is used to set up the aiming reference for each of the nozzles.

g. Grit Blasting the Lines. The lines are applied with the machine spindle running at 0.7 rpm. Grit flow is started when the nozzle is located over the masked portion of the rotor, and grit flow is not turned off until the line is ended at the masked region about the other pole of the rotor.

GYRO MODIFICATION

Rotor Fabrication and Selection

The rotor used in the strapdown Electrically Suspended Gyro is a thin shelled beryllium sphere made from cylindrical billets of I-400 beryllium material. The manufacturing process is outlined as follows:

a. The billets are cut into lengths required for fabrication of the rotor hemispheres.

b. The inner ellipsoidal cavity is machined into the cylindrical parts.

c. Two hemispheres are welded together to form a leak-tight rotor blank.

d. The outer spherical surface is turned.

e. The rotor is ground, lapped and polished in successive operations which bring it to the required size, balance and surface reflectivity.

The two rotors fabricated and patterned under this program are described below:

	Rotor No. 1 Polished Beryllium	Rotor No. 2 Niculoy Plated Beryllium
Diameter	1.99407 inches	1.99395 inches
Mass	20.92 grams	22.08 grams
Sphericity	8 microinches	10 microinches
Moment of Inertia	110 gm-cm^2	114 gm-cm^2

Readout Electronics Modification

The output signal from each optical pickoff is compensated by processing it through a circuit named a Height Insensitive Trigger (HIT). The time interval measurement between pattern line crossings, which is the basis for the gyro attitude readout scheme, must be accurate and stable. The accuracy of the measurement is mainly governed by the consistency with which the pickoff signals can start and stop the time interval counters.

Reflectance variations in the pattern and changes in lamp output appear as changes in pickoff output pulse height. If the trigger action occurred at a fixed voltage level, a time interval error ΔT would occur due to the change in pulse height. The method used to overcome this error is to make the trigger device sensitive to a fixed percentage of height rather than to a fixed voltage; the trigger device is called Height Insensitive Trigger. The basic operation is as follows.

The input pulse is amplified; the amplified pulse is sent to a peak level sensor which samples the peak voltage (flat top) of the input pulse and holds it. The amplified input pulse is then subtracted from one-half of the output of the peak level sensor. The zero-volt crossing of the resultant signal is a fixed percentage (50) of the incoming pulse height. The zero-crossing signal is amplified to increase the slope of the zero crossing, and the zero crossing is then sensed by a tunnel diode threshold detector circuit. The trailing edge of the output pulse is the time mark used to control the time interval counters. The input pulse is differentiated and clipped, amplified, and used to discharge the voltage level sensor so it can accurately sample the peak voltage of the next input pulse.

One of the program tasks established was improvement in response of the Height Insensitive Trigger. The action of the tunnel diode threshold detector circuit was inconsistent as far as comparative switching time between channels in the gyro as originally built; the switching time varied from 50 to 100 nanoseconds. An improvement goal established within the program was to constrain the switching time of each of the three channels to 50 nanoseconds maximum. The part of the HIT cricuit which controls the rise times of the output pulse is shown in Figure 9.

Q4A and CR1 form a transistor-tunnel diode hybrid switching circuit and Q4B is an emitter follower amplifier furnishing low impedance capable of driving a high cable capacitance.

The switching action of Q4A and CR1 can best be explained by looking at the V-I characteristic of the tunnel diode, base-emitter junction of the transistor and the parallel combination of the two (Figure 10). The V-I characteristic has been shifted to the right by the voltage drop across the diode CR3. The shift was required to move the tunnel diode which is a germanium device into the operating region of the silicon transistor.

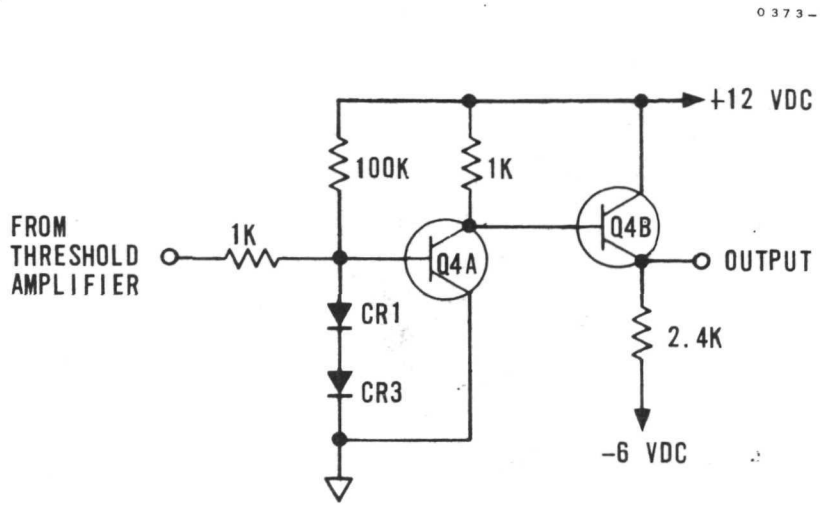


Figure 9. Portion of the Height Insensitive Trigger Circuit

When the signal at the base of transistor Q4A is greater than +0. 55 volt, the tunnel diode switches to its high voltage state and turns on Q4A. The switching action of the tunnel diode drives the transistor from its cut-off region to its saturation region. This switching action determines the rise time for the heading edge of the output pulse which is typically 40 to 50 nanoseconds.

When the signal at the base of Q4A is less than +0. 7 volt, the tunnel diode switches back to its low voltage state. At the time the tunnel diode returns to its low voltage state, the transistor has already left its saturation region and is well into its active region. Therefore, the switching action of the tunnel diode does not influence the speed at which Q4A turns off as much as the triggering signal at the base of Q4A. The rise time for the trailing edge is typically 100 nanoseconds. The difference in rise times for the leading and trailing edges is the inefficient use of the tunnel diode in going from its high voltage state to its low voltage state.

The goal established was to shorten the trailing edge rise time to become comparable with the leading edge rise time of 50 nanoseconds. To accomplish this, the tunnel diode must have a greater influence in turning off Q4A. The tunnel diode has to switch the transistor before it enters the

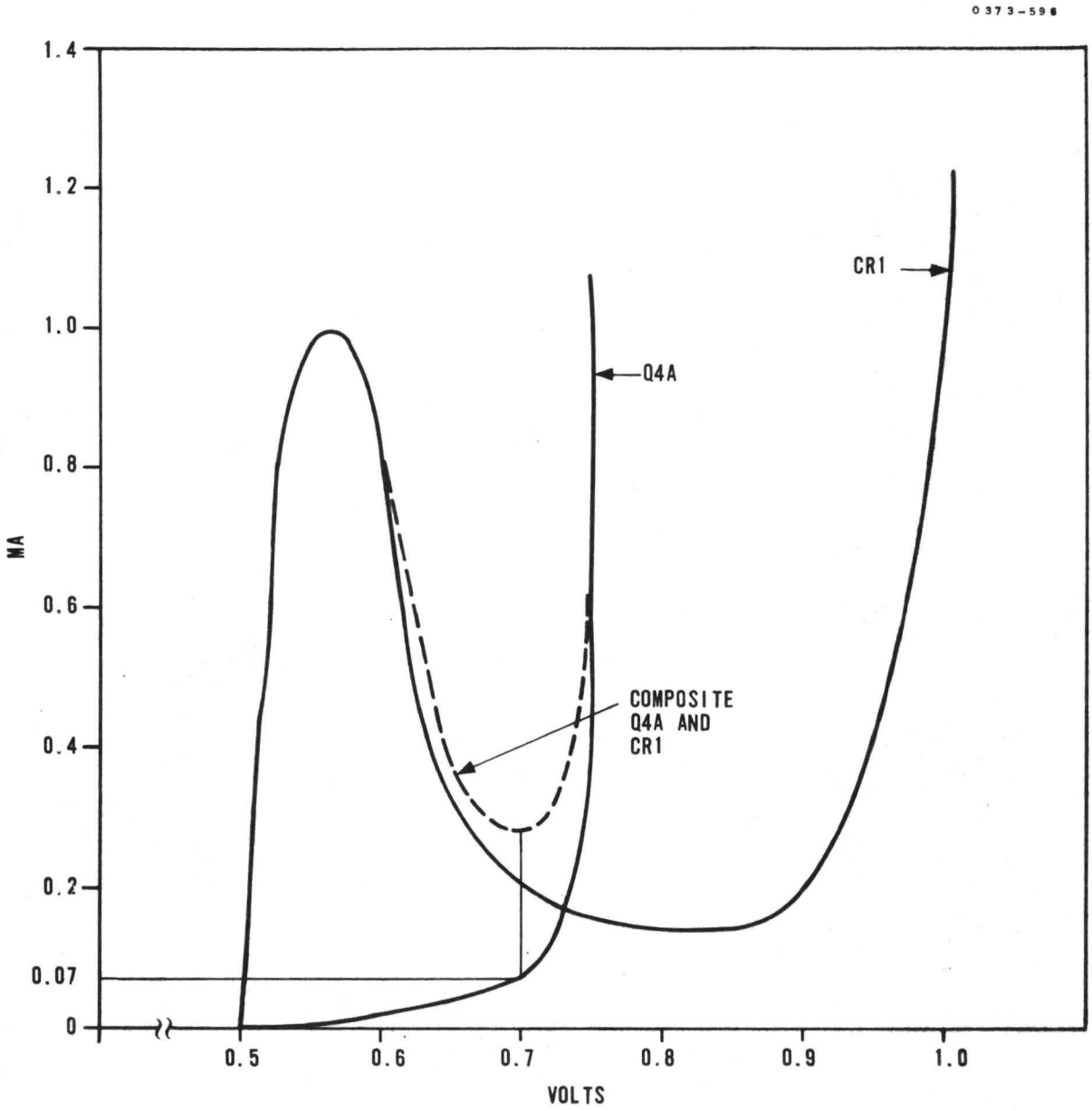


Figure 10. Switching Curve for Original HIT Circuit

active region (the base current must be greater than 110 μa). From Figure 10, the base current is 70 μa when the tunnel diode switches and does not meet the above requirement.

Changing the slope of the base-emitter V-I characteristic will effectively cause the tunnel diode to switch at a greater base current. Figure 11 shows the change in the V-I characteristics when a 300 ohm resistor has been placed in series with the base of Q4A. The base current is now 120 μa when the tunnel diode switches.

A circuit with the base resistor added was compared with the switching circuit of Figure 9. The rise time of the circuit with the base resistor is 45 nanoseconds while the rise time for the actual HIT circuit is 90 nanoseconds. The base resistor for this case was 200 ohms.

The three HIT circuits of the strapdown ESG electronics set were modified by the addition of a resistor placed in series with the base of Q4A. Since the exact value of the resistor depends on the V-I characteristics of Q4A, CR1, and CR3, the resistor was selected for each channel. The rise time for the trailing edge for Y and Z channels is now 40 nanoseconds and X channel is now 50 nanoseconds. The rise times before the modifications were 50 nanoseconds for the Y channel, 110 nanoseconds for the Z channel, and 90 nanoseconds for the X channel. All the rise times are now less than 50 nanoseconds and are within 10 nanoseconds of each other.

GYRO ASSEMBLY AND CHECKOUT

Description of Gyro Assembly Steps

All parts of the gyro are cleaned and prepared for assembly in an environmentally controlled "clean" room. In the initial assembly step, the adsorption type vacuum pump is mounted to the pump-out port on one envelope half; the interface between pump and envelope is sealed with a soft gold ring. Next, the rotor is installed in the spherical inner cavity formed by the two envelope halves; a vacuum tight seal between envelope halves is provided by partially crushing a soft gold wire ring which circumscribes the cavity.

A "pinch-off" tube is mounted outboard of the adsorption pump; this tube is initially connected to a Varian vacuum pump, and it is later "pinched-off" to form a cold weld which is a vacuum tight closure. The "pinch-off" operation disconnects the Varian pump, and the gyro vacuum is thereafter

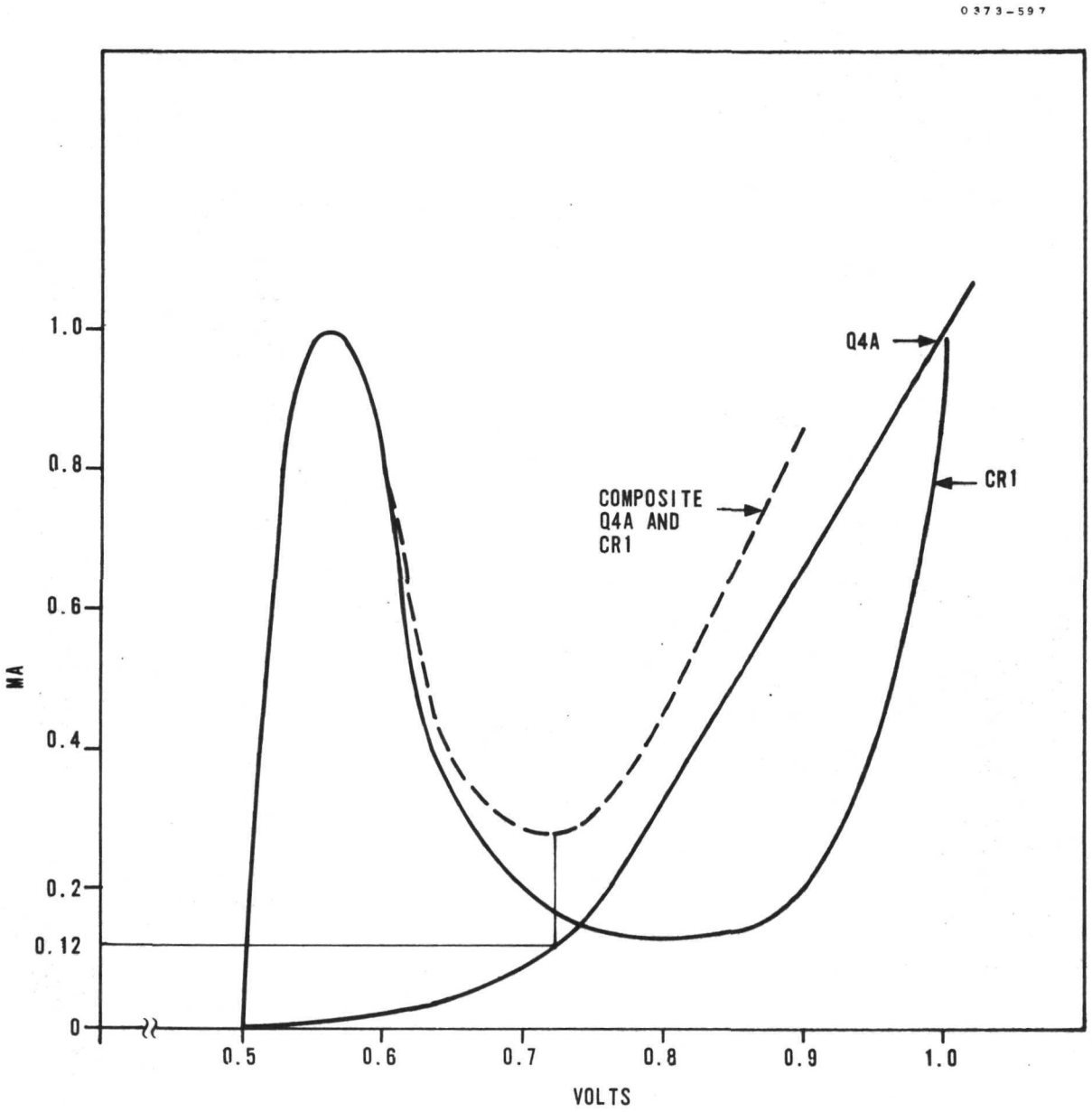


Figure 11. Switching Curve for Modified HIT Circuit

maintained by the integral adsorption pump. While the relatively high capacity Varian vacuum pump is still attached the pumpdown operation is begun; the end requirement of this operation is to achieve a vacuum level of 5×10^{-8} Torr or better as read at the gyro vacuum gage/pump. When the vacuum level passes through 1×10^{-5} Torr, the rotor-envelope-pump assembly is heated to 225°F, and the bakeout/pumpdown operation is continued. When the outgassing rate has decreased to the level compatible with the pumping capacity of the adsorption pump alone, the Varian pump is pinched-off and disconnected.

The optical pickoffs, spin coils, damping coil and other gyro mounting parts are attached to the envelope assembly. Next, this envelope assembly is installed in the gyro mechanical assembly mounting frame, and suspension voltage leads are attached to the envelope electrode pins. The magnetic shields and outer covers are installed. The suspension electronics package is joined to the gyro assembly by means of separate power and signal cables with locking connectors. This completes the assembly of the strapdown electrically suspended gyro which is shown in Figure 12.

Use of a Tooling Gyro in Initial Checkout

Both the suspension electronics and the gyro mechanical assembly were checked out and adjusted as separate assemblies; a static capacitive load was used in suspension electronics adjustment. Although not originally planned, an intermediate form of checkout means was prepared and utilized. The second GFE gyro was sealed and pumped down to operating vacuum level; this gyro was used as a dynamic load with which to test and exercise the suspension electronics. The use of this gyro for an intermediate checkout means was fortunate because its rotor could not be lifted on the initial attempts. The possible causes were considered and a plan for investigation was organized. One of the possible problems was that of breakdown in the coaxial cables which connect the output terminals of the suspension electronics to the gyro electrodes. A test of these insulated cables showed that several developed corona at the voltage levels required for initial pickup of the rotor; this is the highest voltage gradient at which the gyro is operated. Apparently, the dielectric material in the cables had dried and cracked so that its corona resistance had diminished relative to its original rating. Three new cables were manufactured so that a set of six voltage-rated cables could be assembled from the old cables, which had passed the corona test, and from the new cables. The rotor of the intermediate test gyro was then suspended; trim adjustments and tuning were made on the suspension electronics. The same set of six connecting cables was transferred to the gyro assembly containing the new patterned rotor; this set of cables was used throughout the pattern calibration and readout tests conducted with the gyro.

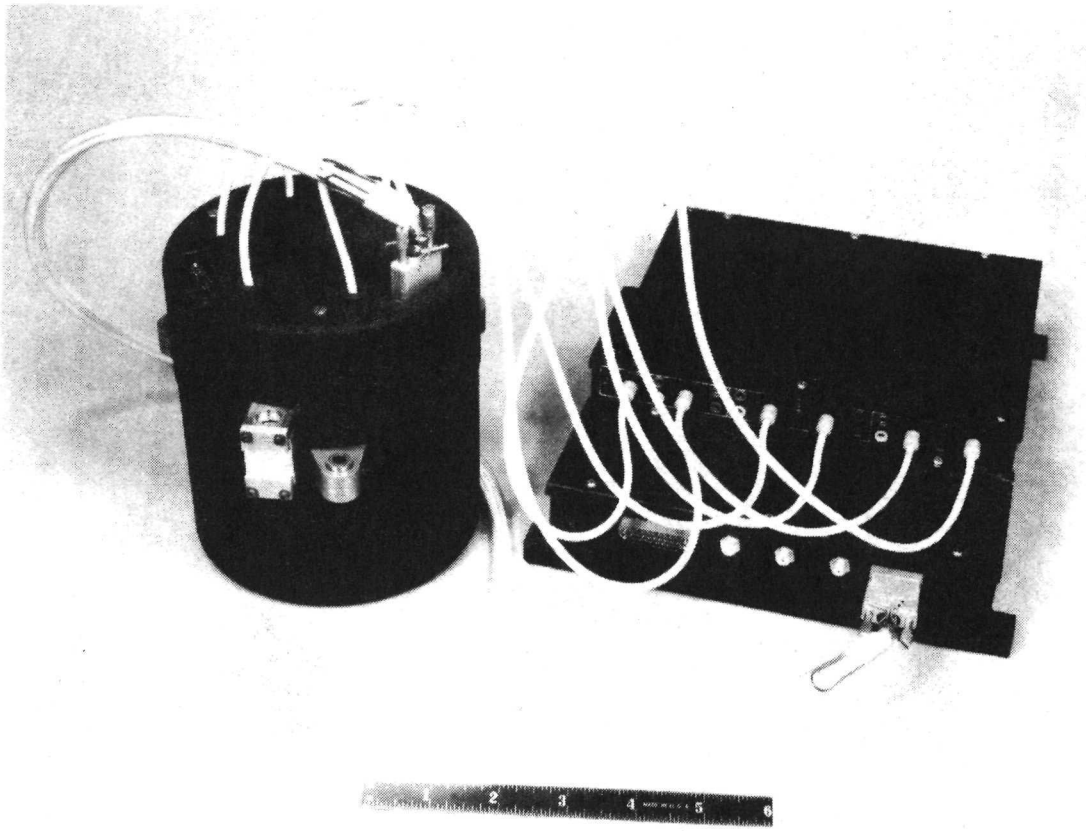


Figure 12. Strapdown Electrically Suspended Gyro

Preparation of the Test Gyro

Loop gain of each channel of the suspension electronics was set to the prescribed level which provides a 4.5 volt (p-p) signal across each channel feedback capacitor. In addition, a transient response test was conducted by applying a 10 Hz square wave to the designated test points in the suspension electronics; this provides displacement forces acting on the rotor. Proper damping of the feedback capacitor signal in each channel was observed upon removal of the forcing voltage.

During the pre-spin checkout of the gyro, the original pickoff lamps burned out. Exact replacement lamps were not available for immediate installation so a compromise was made on lamp substitution. Lamps which were available and which would fit into the small mounting volume allocated gave approximately one-half the illumination and pickoff signal output of the original lamps. The original pickoff signal output is very desirable in terms of attaining the best readout accuracy, but an attenuation factor of two was accepted, rather than delay the gyro test by several weeks for the procurement of original equipment lamps.

The rotor was suspended and spun up to about 10 rps; the gyro was monitored for about 20 hours with the rotor continuously suspended as a confidence check. No suspension problems were encountered. The rotor was then spun up toward the planned speed of 500 rps. The feedback signals of the gyro are monitored during initial spin-up, and they gave evidence of an unexpected problem. Modulation of the feedback suspension signals at the rotor spin speed grew more rapidly than normal, and spin-up was stopped at 300 rps with the feedback signals modulated near 100 percent. A check of rotor rundown rate showed abnormally high rates which confirmed a high radial mass unbalance in the rotor. A check with the rotor manufacturing group brought to light an unfortunate omission which occurred during fabrication of the experimental Niculoy-plated rotor; the rotor balance was not measured and adjusted to the requested 0.2 dyne-cm level concurrent with grinding and lapping to final size. The radial unbalance of the Niculoy-plated rotor came out to be about 15 dyne-cm as calculated from measured rundown rate and known suspension electronics parameters. This very high unbalance occurred because of an omission in the planned rotor fabrication process; it will not be a problem during the build of additional gyros of this type.

Since the rotor unbalance was not measured and corrected after Niculoy plating, the axial mass unbalance component of total mass unbalance was also much higher than planned. The limit requested on axial mass unbalance

was 0.2 dyne-cm; the actual value is 11 dyne-cm based upon rotor drift measurements. The presence of greater than expected rotor drift complicated the procedure of pattern calibration. This will be discussed more fully in the paragraphs which describe the calibration procedure. The effect of high rotor unbalance observed during the initial spin-up toward the planned running speed was that of rotor "wobble" as the rotor tended to spin about its mass center. In order to provide adequate safety margin in terms of suspension signal modulation, all pattern calibration and readout signal data was recorded after running up the rotor to an initial speed of 250 rps. The calculated range of usable rotor speed for readout purposes is 200 to 500 rps with the high limit constrained by the microcreep properties of the beryllium rotor material. Readout accuracy should be slightly better at the high side of the allowable speed range because of the faster waveform transition as the optical pickoff senses the passage of the pattern trailing edge. Pattern calibration and readout accuracy should be even more accurate on future gyros which can be calibrated at a rotor speed of 500 rps.

Mirror and Pickoff Alignment

The pickoff alignment procedure requires the use of two reference mirrors securely attached to the gyro envelope. The mirrors are nominally orthogonal to each other; each mirror is further constrained so that a normal to its surface is parallel to the imaginary line passing through the center of the suspended rotor and the center of the objective lens of its associated optical pickoff. The area of mirror attachment to the envelope is on a diameter across the envelope from the associated pickoff.

The pickoff alignment procedure is conducted with the gyro mounted on a precision single axis table and dividing head; the table axis is vertically aligned, and the gyro is initially positioned so the normal to one reference mirror is parallel to the table axis. The gyro (mirror) alignment to the table axis is checked by rotating the table and observing the "coning" angle read from the mirror face. The gyro attitude is shimmed to reduce the mirror "coning" angle to three arc-seconds or less. With the gyro attitude unchanged, the optical pickoff which is on the vertically oriented axis is loosened and translated by means of a special fixture to reduce its "coning" angle output to the equivalent of 15 arc-seconds or less.

After the first pickoff has been aligned, it is fastened down to the envelope mounting pads, and the "coning" operation is repeated to assure that excessive translation did not occur during the fastening step. The procedure

is then repeated in order to align the second optical pickoff. The procedure is modified slightly for the alignment of the third pickoff which is adjusted (by means of the coning angle measurement of output) to be perpendicular to the plane determined by normals of the two orthogonal reference mirrors. The exact angle between the mirrors is measured for use in the calibration program; the angle between mirrors on this gyro is 89 degrees, 56 minutes and 5 seconds.

PATTERN CALIBRATION AND READOUT ACCURACY

Pattern calibration involves operating the gyro in a series of planned tests to gather the required data which consists of pickoff output, time, envelope attitude, etc. The gyro is mounted on a stable pier with a precision dividing head as an intermediate member. Gyro output data is recorded through a test station data processor. A detailed discussion of the procedural considerations and a description of the equipment and process is given in the following paragraphs.

Calibration Data Samples

The data utilized for calibrating the pattern mechanization equation were samples taken in five-, two-, and one-degree increments, as measured on the angle scale of the dividing head spindle axis. The gyro was mounted on the dividing head plate for the calibration operation; the rotor spin vector was oriented so that its drift with respect to Earth-fixed coordinates was at a minimum.

The five-degree increment samples were taken over the entire pattern range. The smaller increment increment samples were collected at the pattern range extremities. Earlier studies had shown the need to gather finer resolution data samples at the pattern extremities in order to obtain the most accurate, overall pattern compensation.

The two-degree samples overlapped the five-degree samples over those pattern areas greater than thirty degrees from the equator, and the one-degree samples overlapped the five- and two-degree samples over those areas greater than forty degrees from the rotor equator.

Considerations of Calibration Procedure

The procedure followed for taking the calibration data was established by the need to accurately measure the angle between the viewing axis of the pickoff used to collect the calibration samples and the rotor spin vector. The scale on the dividing head spindle axis provides a means of incrementing the gyro envelope attitude to an accuracy of two seconds or less. During the collection of the five-, two-, and one-degree samples, the gyro envelope was rotated by these increments as measured on the dividing head spindle scale. To accurately establish the pickoff axis-spin axis angle for each data point, several other factors were taken into account:

- Establishment of a baseline or reference attitude from which the angular increments are measured.
- Selection of a mounting relationship between the gyro envelope (and optical pickoffs) and the dividing head axes.
- Minimizing the gyro drift due to axial mass unbalance during the calibration data recording period.
- The compensation for residual gyro drift effects in the recorded data.

Determination of a baseline angle. - Establishment of a baseline angle consists of accurately relating a specific pickoff axis to spin axis angle (hereafter denoted as the colatitude angle) to a specific attitude count ratio. Several baseline angles are available when the angle between two pickoffs is known. A simple example is one where the case is positioned so that the spin vector lies in the plane of two pickoffs. The gyro case is oriented about the axis orthogonal to this plane so that the count ratios of these two pickoffs are equal. The spin vector then bisects the angle between the pickoffs. Actual usage of this angle as a baseline is subject to potential error sources: one is the uncertainty in pickoff alignment parameters from which pickoff angles are determined; another is the error incurred if the spin axis is not actually in the intended coordinate plane.

The latter error would not be a factor for a baseline established where the count ratios from all three pickoffs are equal. Knowledge of the pickoff alignments permits a computation of the colatitude angle related to it. If, for example, the pickoffs are exactly orthogonal, the angle is arc-cos $\sqrt{1/3}$ = 54.73561 degrees, by virtue of the direction cosine orthogonality identity.

The pickoff alignment uncertainty can also be removed as an error factor for a convenient baseline point by recognizing the fact that two colatitude angles exist such that all three count ratios are equal, and that these points are symmetrically located from the equator. If the angle between these points is bisected, one can determine what the count ratio is for the rotor equator. The primary uncertainty develops from the bisecting process; however, this can be maintained to a tolerable level by minimizing the spin vector drift during bisection.

Selection of an envelope mounting relationship. - When the dividing head spindle is rotated five degrees, some means must be available to relate this to the colatitude change of the pickoff recording the calibration data. A one-to-one scaling relationship is the easiest and most uniform one to use; such a scaling results if both the spin axis and the axis of the pickoff used for calibration are orthogonal to the dividing head spindle axis. One pickoff can be set parallel to the spindle by first aligning the pickoffs, then mounting and aligning the gyro case so that the normal of one of the reference mirrors is parallel to the spindle axis. The other pickoffs are then orthogonal to the spindle axis; either one can be used for collecting the calibration data. The spin vector is placed orthogonal to the spindle axis by orienting the spindle axis direction so that the count ratio from the pickoff set parallel to the spindle axis is equal to the equatorial baseline ratio.

Cancellation of unbalance drift effect. - The greatest potential error source is spin vector drift while calibration data or any preliminary measurements are being made. The spin vector of an ideal, torque-free gyro is stabilized in inertial space; it could be stabilized in Earth-fixed coordinates as well by aligning it along the Earth's polar axis (EPA). Mass unbalance torque will cause the actual ESG rotor to drift from the EPA in a horizontal direction. Better Earth-fixed stability can be achieved by aligning the spin vector sufficiently above or below the EPA in the north-south vertical plane so that the resulting mass unbalance drift is cancelled by the movement produced by the Earth's rotation. During the acquisition of calibration data, the samples were taken with the spin vector stabilized in this way.

Residual drift correction. - With the axial unbalance drift canceled by a suitable EPA offset, a small drift will still occur during the calibration sampling. This drift is primarily caused by a combination of:

- Electric torque, which varies according to the orientation of the spin vector relative to the case.

- High rundown rate. By the resulting change in momentum, the mass unbalance drift would change causing incomplete cancellation of spin vector movement from Earth's rotation.

The estimation of and compensation for the drift occurring during the calibration scans is an important factor in determining the procedure for obtaining and reducing the calibration data. All of the scans begin with a sample of counts at or near a baseline angle around which the count ratio as a function of colatitude angle is known in some detail. A calibration data scan is then made over the pattern region of interest. After the scan is completed, the dividing head spindle is returned to the baseline position. The observed change in count at the baseline point before and after the scan is used to estimate the drift which occurred during the scan. An interpolation of drift angle on the basis of time is then made for each data sample in the scan; since the station clock time is recorded with each sample, such an interpolation can be made with good accuracy.

This technique is accurate if the drift rate is constant for the duration of the scan. The direction and magnitude of electric torque, however, is a function of the spin axis orientation in the gyro. This is an uncertainty factor in the drift interpolation technique. Data scans involving a relatively wide pattern range or a large number of increments are particularly vulnerable to this factor which is reduced by limiting the number of increments. In areas where greater accuracy is required, "localized" scans (in the sense that the spin axis-case axis orientation changes by a relatively small amount over the major time portion of the scan) will minimize the drift variation. This is an important purpose served by the two-degree and one-degree scans at the extremities.

The need to estimate and compensate for drift with a minimum of error suggests that the optimum location of the baseline point at which the scans are started is at a central point of the patterned region, and that the change of count ratio be a relatively linear function of colatitude angle in that region. The use of the rotor equator as a base point serves this purpose well in both of these respects. Detailed knowledge of the count ratio function in the equatorial region is provided by a ten-minute increment scan over an angle of one degree on each side of the equatorial region.

All of the scans use the equatorial baseline as the starting point. The two-degree band over which the count ratio function is detailed serves as a common denominator for correlating the colatitude angle determinations for all the wider range data scans.

Calibration Data Acquisition Procedure

The equipment used to calibrate and to measure the readout accuracy of the Strapdown ESG is listed below:

- Leitz Dividing Head
- Adapter plate and fixture for mounting the gyro to the dividing head
- Single axis turntable with rotation axis aligned vertically
- SDESG Gyro Control Console
- SDESG Data Processor
- Theodolite.

The test setup and operating procedure is outlined as follows:

1. Mount the gyro onto the dividing head plate using the adapter plate and fixture so that one of the gyro reference mirror normals is parallel to the spindle axis. Shim the mounting to null the coning of the mirror normal, as the gyro is rotated, as viewed through the theodolite.

2. Align the damping coil axis parallel to the EPA. Perform the gyro starting procedure to bring it to its normal operating condition.

3. Determine the gyro drift rate out of the North-South vertical plane. Offset the spin vector from the EPA but in the North-South vertical plane, so that this drift is canceled by Earth's rotation. Determine the drift again and readjust the offset, if necessary.

4. Position the gyro case with respect to the spin vector so that the C_1 counts from all three pickoffs are as nearly equal as possible within limits of adjustment. Repeat for the opposite rotor hemisphere.

5. Reposition the table and tilt axes so that the spindle axis is nominally perpendicular to the spin axis.

6. Measure the angle between the averaged count ratios obtained in Step 3 by positioning one of the pickoffs at each of the count ratios obtained and reading the spindle axis scale at each setting.

7. Position the same pickoff midway between the two settings of Step 5. This should establish the count ratio at the equator. To reduce the effect of drift, it may be necessary to repeat this and the previous step.

8. Reposition the turntable and/or tilt angle position so that the pickoff aligned along the spindle axis reads the count ratio determined in the previous step. Lock down the table to prevent any inadvertent movement during the calibration scans. Prior to Steps 10, 11 and 12, the tilt angle should be readjusted to reposition the gyro so that this pickoff reads the equatorial count ratio.

9. Scan the pattern one degree on each side of the equatorial count ratio position in 10-minute increments. Start and end with the same spindle axis setting to provide a correction for drift.

10. Scan the entire pattern in five-degree increments. Start at the equatorial count ratio position and scan to one extremity, and return to starting spindle axis setting. Repeat to the other extremity.

11. Readjust starting position at the equatorial count ratio. Rotate spindle axis 30 degrees and scan in two-degree increments to the end of the pattern. Return to starting spindle position at equator. Repeat to the other extremity.

12. Readjust starting position at the equatorial count ratio. Rotate spindle axis 40 degrees and scan in one-degree increments to the end of the pattern. Return to starting spindle position at equator. Repeat to the other extremity.

13. Shut down gyro and reduce data. Only the five-, two-, and one-degree data are used in regressing for coefficients; it is first corrected for spin vector drift, using a linear interpolation with time. Drift during each scan is estimated from the change in count ratio for the identical dividing head settings at the beginning and end of each scan with the aid of the 10-minute increment scan obtained in Step 9.

SDESG Data Processor Description

The UG1989A1 Data Processor contains the logic, switching and accessory equipment necessary to automatically read and record data from the gyro. The Data Processor is composed of two racks; the logic rack and the output rack. The output rack holds the Soroban punch and the Friden flexowriter. The logic rack holds two high speed counters, a digital voltmeter, precision frequency standard,two panels with logic and control functions and two power supply panels. The data processor racks appear on the left-hand side of Figure 13; the gyro control console is in the middle, and the gyro, installed on the Leitz dividing head, is on the right-hand side. Time between gyro pickoff pulses is measured by the two 100 MHz time interval counters. The 100 MHz timing signal is derived from a 1 MHz precision frequency standard. The pickoff pulses are used to start and stop the 100 MHz timing signal going to the high speed counters.

Information from the counters is then fed to the Soroban and punched on paper tape. The paper tape is then fed to the flexowriter and a typed printout is obtained.

The FCG 169A2 control console contains power supplies and controls necessary to operate the gyro. The console monitors gyro pressure and meters all gyro and suspension input current and voltages.

The gyro rotor spin-up current is produced by a two-phase variable frequency oscillator and power amplifier. The two-phase current is then fed to a "Scott-Tee" transformer which produces the required three-phase current.

Damping and pickoff lamp currents are produced by variable dc power supplies. A variac and isolating transformer control the 60 cps degauss current.

The suspension power supply provides ±22 volts dc, +12 volts dc and -6 volts dc for the suspension electronics. Pickoff preamplifiers and HIT (Height Insensitive Trigger) circuits are powered by lines decoupled from the suspension supplies. Suspension supplies include backup batteries, which switch in automatically in an emergency. Fast and trickle charge circuits are built in.

The gyro vacuum pump is operated automatically by a Veeco ionization gage controller. The pump getter evaporation power is supplied by an adjustable 0 to 1000 dc, 20 ma power supply.

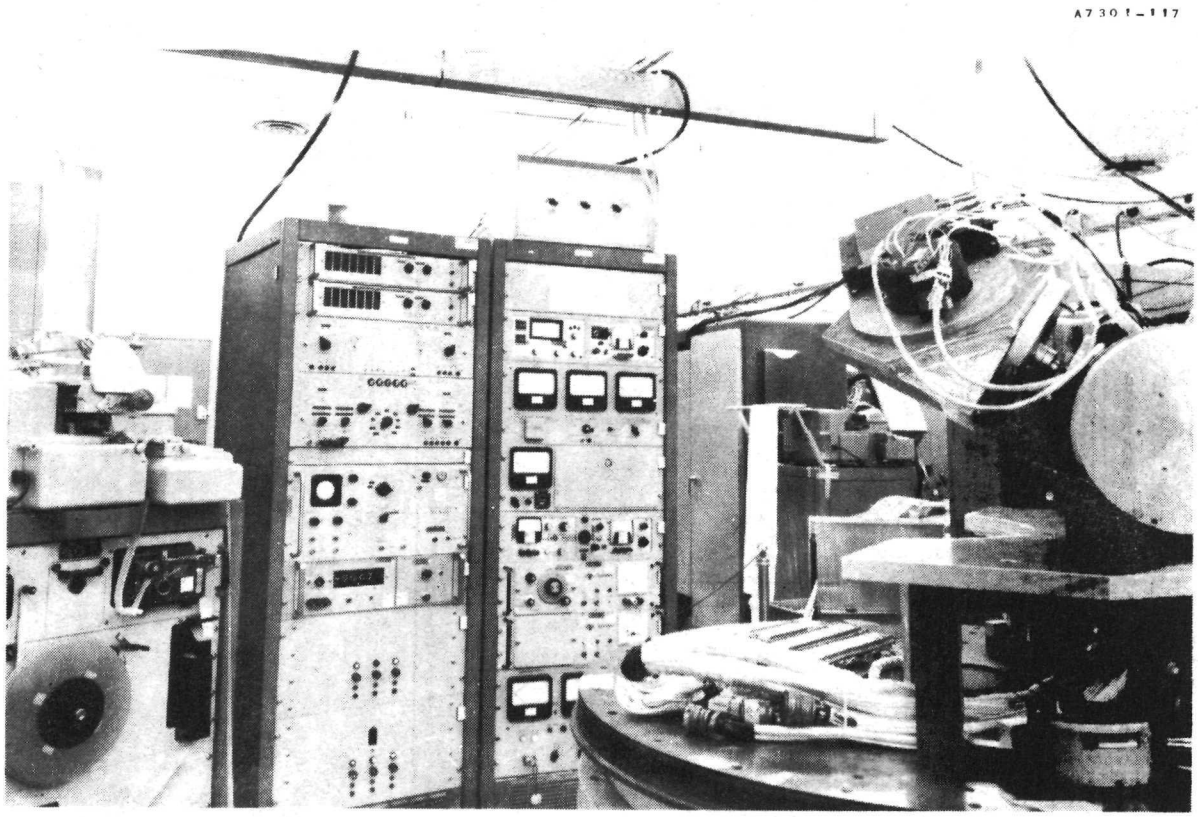


Figure 13. Laboratory Equipment

Before data taking, several adjustments on the gyro and data processor were made to improve pulse quality, remove noise pulse and reduce data scatter.

To reduce scatter in the data, three potentiometers were mounted on the gyro to control the individual lamp currents. By adjusting the lamp currents, the height of the pickoff pulses can be made uniform, which reduce discrepancies between pickoffs. The three pickoffs were adjusted to give a height of 2.1 vpp (this is the minimum height of the three before adjustment).

The HIT circuit contains a threshold adjustment which discriminates against pulses from the pickoffs which are less than a predetermined value. The pulses from the pickoffs were 2.1 vpp and the threshold adjustments were set to permit passage of pulse of amplitude 1.5 vpp or greater.

The data processor has two adjustments for eliminating false data points due to extraneous noise pulses (predominately due to arc marks). The pulse width discriminator requires all pulses coming from the HIT circuit to have a minimum width. This width is adjustable between 2 and 24 microseconds. The gyro is spun up to operating speed and attitude such that one pickoff is looking at the very extremity of the pattern. The pulses at this point will be at their widest. The pulse width discriminator is adjusted to a point just before the pulse disappears.

The second adjustment is the delay on a delay multivibrator which controls the time in which the pattern pulse must follow the logic line. If the pattern pulse does not follow the logic line in the predetermined time unit (the delay time of the multivibrator), the start pulse will not be gated to the high speed counters. The gyro is spun up to operating speed and position so a pickoff is looking at the extremity of the pattern. The time from the trailing edge of the logic line to the trailing edge of the pattern line is measured and the delay of the multivibrator is adjusted to be this time plus 20 microseconds.

The data processor has the ability to sum counts over 1, 2, 4, 8 and 10 revolutions of the rotor. To acquire the desired resolution between counts, the data processor was set to sum over 10 revolutions of the rotor. The data period (time between successive data points) was set to 0.0002 hour to minimize changes due to drift and rotor run down.

Pattern Mechanization Equation

General form of pattern lines. - The great circle pattern was selected for use on the test rotor in this readout improvement program. A parametric representation of a great circle is

$$a \sin\theta \cos\phi + b \sin\theta \sin\phi + c \cos\theta = 0$$

since the intersection of the surface of a unit sphere and a plane bisecting the sphere is a great circle. In this equation, the parameters (a, b, c) are the direction cosines of the axis normal to the plane with respect to a set of cartesian coordinates (x, y, z), respectively. Spherical polar coordinates are used to describe the spherical surface: θ is the polar or colatitude angle; and ϕ is the azimuth or longitude angle. The transformation from cartesian to polar coordinates is given by

$$x = r \sin\theta \cos\phi$$

$$y = r \sin\theta \sin\phi$$

$$z = r \cos\theta$$

where r is the radial distance from the origin. The unit sphere is described by setting r = 1.

The pattern lines on the rotor have a finite width; it also should be realized that errors develop in tool setup in preparation for the grit blast used to apply the pattern line. These factors cause the line edge to deviate from a great circle segment to a minor circle segment. However, a minor circle segment on a unit sphere can be described by the same form of equation; namely,

$$a \sin\theta \cos\phi + b \sin\theta \sin\phi + c \cos\theta = d$$

where d is the distance of the intersecting plane from the center of the sphere.

The patterning procedure followed is one that maintains (a, b, c) to be the same for all line edge segments applied to the rotor. The finite width results in a different value for d for opposite edges of one pattern line; the difference in these two values, however, is equal to the ratio of the line width to the radius of the sphere.

The trailing edge of each line segment is used for triggering the time interval measurement counters. The trailing edge of the first pattern line

is defined by one end of the nozzle and the trailing edge of the second pattern line is defined by the opposite end of the nozzle. Consequently, the line edges of interest are segments of different minor circles whose defining planes are parallel and separated by the width of the grit nozzle used for applying the pattern lines. This distance is equal to 0.060.

Since the defining planes for the line edges are parallel, some simplifications are possible in the equations which describe them. The general equation includes a degree of rotational freedom about the pole (spin axis) which is not of concern. The orientation of cartesian coordinates about this axis is therefore arbitrary; it is consequently chosen so that the axis orthogonal to the defining planes lies in the Y-Z plane. As a result,

$$a = 0$$

The equatorial crossing of the line edges occurs approximately at $\phi = 0$ for line 1, and at $\phi = \pi$ for line 2; they deviate from these values by the line edge and the errors in the line application tool setup.

Taking these factors into account, the pattern lines can be described as segments of two equations. For line 1,

$$b \sin\theta \sin\phi + c \cos\theta = d_1; \text{ for } -\frac{\pi}{2} < \phi < \frac{\pi}{2} \qquad (1)$$

For line 2,

$$b \sin\theta \sin\phi + c \cos\theta = d_2; \text{ for } \frac{\pi}{2} < \phi < \frac{3\pi}{2} \qquad (2)$$

Phase Angle Information. - The trailing edge of the two pattern lines is used to trigger start and stop gates of clock pulses which give a measurement of the time interval between the start and stop trigger pulses. Two time interval measurements are recorded: one between the trailing edges of line 1 and line 2; and one between consecutive pulses generated by the edge of line 1. The latter is a measurement of rotor period; its reciprocal yields the rotor spin speed. The ratio of the former to the latter is a measurement of the phase angle between the line edges; from knowledge of the equations of the line edges, the colatitude or direction cosine can be calculated.

For a given colatitude, let the longitude coordinate of lines 1 and 2 be denoted by ϕ_1 and ϕ_2', respectively. The phase angle from the readout is given by

$$\mu = 2\pi \left(\frac{C_1}{C_1 + C_2} \right)$$

where C_1 is the time interval measurement from line 1 to line 2, and $(C_1 + C_2)$ is the rotor period measurement. This phase angle is related to the longitude intercepts by

$$\mu = \phi_2' - \phi_1 \tag{3}$$

The nominal mechanization equation can now be derived from this expression and the equations for the line edges.

Derivation of the nominal mechanization. - Since,

$$\sin x = \sin (\pi - x)$$

it is convenient to set

$$\phi_2 = \pi - \phi_2'$$

and thereby restrict our interest only to the primary values in the inverse trigonometric functions of ϕ_1 and ϕ_2. The phase angle relationship of Equation 3 becomes

$$\mu = \pi - \phi_2 - \phi_1$$

or

$$\phi_1 + \phi_2 = \pi - \mu \tag{4}$$

The pattern line Equations 1 and 2 need now to be restated as a solution for ϕ_1 and ϕ_2. For line 1

$$\phi_1 = \sin^{-1} \left(\frac{d_1 - c \cos \theta}{b \sin \theta} \right) \tag{5}$$

while for line 2

$$\phi_2 = \sin^{-1}\left(\frac{d_2 - c\cos\theta}{b\sin\theta}\right) \tag{6}$$

Consider the trigonometric identity

$$\sin\phi_1 + \sin\phi_2 = 2\sin 1/2(\phi_1 + \phi_2)\cos 1/2(\phi_1 - \phi_2)$$

Substituting Equations 4, 5, and 6 into the identity yields

$$\frac{d_1 + d_2 - 2c\cos\theta}{b\sin\theta} = 2\sin 1/2\,(\pi - \mu)\cos 1/2(\phi_1 - \phi_2) \tag{7}$$

The last factor on the right hand side involves ϕ_1 and ϕ_2 which are approximately equal (compare Equations 5 and 6); consequently this factor is nearly unity. By a rather lengthy derivation involving trigonometric identities and square root approximations, it can be shown that

$$\cos 1/2\,(\phi_1 - \phi_2) \cong 1 - \frac{(d_1 - d_2)^2}{8(1 - \sin\phi_1 \sin\phi_2)(b\sin\theta)^2}$$

where Equations 5 and 6 can be used to remove $\sin\phi_1$ and $\sin\phi_2$ from the right hand side. For the nominal pattern parameters

$$0.98 < \cos 1/2\,(\phi_1 - \phi_2) < 1.00$$

This approximation can result in a two percent error, but the simplification in the pattern mechanization equation is considered desirable. The polynomial whose coefficients are determined by calibration will correct the above error.

The nominal mechanization will be a solution of the following equation for $\cos\theta$:

$$\sin 1/2\,(\pi-\mu) = \frac{d_1 + d_2 - 2c\cos\theta}{2b\sin\theta}$$

$$= \frac{\bar{d} - c\cos\theta}{b\sin\theta} \tag{8}$$

where

$$\bar{d} = \frac{d_1 + d_2}{2}$$

A first approximation at the solution is obtained by assuming $\bar{d} = 0$:

$$\cot \theta = \frac{b}{c} \sin\left(\frac{\pi - \mu}{2}\right) = \frac{b}{c} \sin \delta$$

$$\cos \theta = \frac{\cot \theta}{\sqrt{1 + \cot^2 \theta}} = \frac{b \sin \delta}{\sqrt{c^2 + b^2 \sin^2 \delta}} \tag{9}$$

The solution for $\bar{d} \neq 0$ can be developed by squaring Equation 8 and utilizing

$$\sin^2 \theta \equiv 1 - \cos^2 \theta$$

and the quadratic formula. Equation 9 is used as a guide to eliminate the extraneous solution introduced by the squaring operation. The exact nominal solution can be written in terms of a perturbation of Equation 9:

$$\cos \theta_n = \frac{b \sin \delta}{\sqrt{c^2 + b^2 \sin^2 \delta}} \sqrt{1 + \frac{\bar{d}^2}{c^2 + b^2 \sin^2 \delta}} + \frac{\bar{d}\, c}{c^2 + b^2 \sin^2 \delta} \tag{10}$$

where the subscript n denotes the nominal value.

Two sources of error can produce repeatable deviations from the nominal mechanization. The first is the potential occurrence of application error; an example of this is lateral runout of the spindle bearing during grit blast. The second is approximation error in deriving the nominal mechanization given in Equation 10. The primary contribution here is the dropping of the factor $\cos 1/2(\phi_1 - \phi_2)$ from Equation 7.

A polynomial series in y, where

$$y = \frac{C_1}{C_1 + C_2} - 1/2$$

was utilized to model the measurable deviation from the nominal mechanization:

$$\cos \theta_m - \cos \theta_n = p_0 + p_1 y + p_2 y^2 + \ldots + p_7 y^7 \qquad (11)$$

This is the number of terms that was effective in reducing the rms error in the pattern calibration residual. Trial solutions with higher order polynomials did not significantly improve the resultant calibration.

Pattern Calibration Software

A computer program was written for the purpose of calibrating the pattern mechanization polynomial coefficients. The program was coded for execution on the University Computing Company's Univac 1108 Computer via a remote terminal located at the Honeywell Aerospace Division. Simulated data points were generated to debug the program before gyro data became available.

Simulation studies. - Weighting of the pattern range extremities was enhanced by providing a greater density of data samples from these areas of the pattern. An additional emphasis on these extremities can be accomplished by a weighted calibration of the polynomial coefficients. The study on simulated data explored the use of the weighting function

$$W(x) = (1 - x^2)^{-1/2} \qquad (12)$$

where x is a linear transformation of y such that

$$-1 < x < 1$$

over the range of y. The major advantage of using this weighting factor over no weighting is that the residual error is uniform over the range of data; with no weighting, the error tends to be greatest at the pattern extremities.

The simulated data samples were used to experiment with a calibration technique utilizing orthogonal polynomials. The Chebychev Polynomials of the First Kind are orthogonal polynomials with respect to the weighting factor given in Equation 12.

If they could be used, a solution for the polynomial series coefficients would be obtained without resorting to a least squares method. Such a method was feasible, however, only if the polynomials formed by the calibration data were indeed orthogonal. Experiments with the simulated data demonstrated

that the Chebychev polynomials so formed were not orthogonal because the data points were not uniformly distributed over x. The procedure for collecting calibration data permits control on the distribution of the colatitude variable θ; however, the independent variable of the mechanization is the count ratio of the data samples resulting from the distribution of θ. The distribution of the count ratio depends not only on the distribution of θ but on the pattern, and to a small extent on the line deviations which are being modeled.

While the least squares method was used to determine the polynomial coefficients, the Chebychev polynomials were still retained in the calibration with the actual gyro data. Retention of the Chebychev polynomial formation was considered beneficial in that the least squares matrix of the Chebychev polynomials would be better conditioned than that of the mechanization polynomial itself.

A problem associated with the weighting factor is that it goes to infinity at the range limits of x. In order that the weighting not be unduly large for the data sample at each extremity, a margin at each end was included in the mapping of the y variable into x. The magnitude of the margin was determined based on trial calibrations on the simulated data; this margin was set to a count ratio equivalent of 0.005.

Computer program. - The program consists of a driver which forms the Chebychev Polynomials, forms the least squares matrix, and transforms the Chebychev coefficients into the form used directly in the mechanization. The driver also computes the residual error for data points used in the calibration and error values for other data points of interest. Two subroutines were provided: one reads the calibration data into the array or generates simulated data, and the other is a standard subroutine for solving the least squares normal matrix.

The computational procedure of the program is as follows:

- Read the calibration points and determine the parameters for mapping y to x.
- Compute the nominal colatitude angle from the great circle mechanization parameters b, c, and d, and subtract it from the input colatitude to form the observed error to be modeled by the polynomial.

- Transform the y variable to the x variable and compute Chebychev Polynomials for each data sample. Use these values for the formation of the least squares matrix for calculating the Chebychev Polynomial coefficients.

- Solve for the Chebychev coefficients, using both the least squares method, and the direct calculation assuming that the Chebychev Polynomials are orthogonal.

- Compute the calibration residual for each data point.

- Using the model thus determined, calculate the readout error for data samples recorded during the pattern calibration scans but not used in the calibration.

Data Reduction Technique. - The nominal mechanization parameters were determined from computations utilizing the two colatitude points at which equal count ratios were provided by all three pickoffs. Two data points are sufficient for the determination of b, c, and $\bar{d}$ because

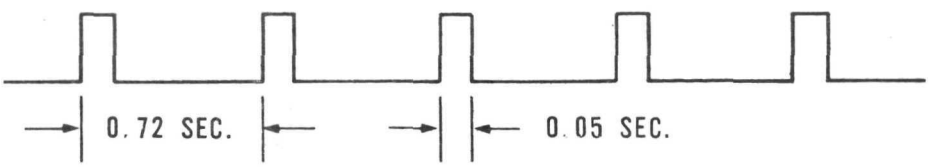
$$b^2 + c^2 = 1,$$

since they are direction cosines. Polynomials ranging from the fifth through the ninth order were calibrated and the residual error was determined. The seventh order polynomial resulted in good accuracy so this was the order of polynomial used in calibrating the actual test data.

Readout Test Results

Readout data was recorded from the gyro in the angular increments described previously in this chapter. At each setting of the dividing head spindle, five successive sets of pickoff output data were read at intervals of 0.72 second. Each of the successive sets punched out was the result of ten successive revolution pickoff outputs read and averaged within the test station data processor. The time base for data recording was:

0373-599



The five sets of data points taken at each attitude served to guard against anomalous behavior on the part of the data processor which is beginning to show some effects of age. In the entire data scan of 275 lines, two data blocks or ten anomalous lines of data were discarded on the basis that either the C_1 or $\frac{C_1}{C_1 + C_2}$ values differed greatly from the average over the remaining lines. The average values of data points differed very little from individual line values corrected for time. The data used in data processing was effectively the average of fifty data points. Ten revolution averaging should be sufficient in the operational use of such a gyro.

The data format as printed out on the test station Flexowriter is shown in Appendix A along with a portion of actual data recorded. The data formats from the pattern calibration and readout accuracy programs as run on the UCC 1108 computer are shown in Appendix B along with the actual data values.

The gyro pattern was calibrated with data selected according to the following schedule:

Data Increment	Range Utilized
5 degrees	Single band centered on the pattern median and extending for 35 degrees on each side.
2 degrees	Two bands of 4 degrees on each side of the central band.
1 degree	Two bands of approximately 5 degrees lying adjacent to the three central bands described above.

The pattern was also calibrated using only pickoff output data gathered at five-degree increments. After calibrating the pattern according to the two schedules described, the data points recorded during test, but not used in the calibration schedule, were used in the computation of readout accuracy.

The results of the pattern calibration and readout accuracy tests are shown in Table 4.

The error in calibration at each measured data point was calculated; this is a part of the data shown in Appendix B. The separate error values were also combined in computations of rms and averages of absolute value. The

TABLE 4. PATTERN CALIBRATION AND READOUT

Pattern Calibration Results - Summary

Data Set	Number of Data Points Recorded *	RMS Value of All Calibration Error Amounts	RMS Value - Percentage of Accuracy Goal	Average Absolute Value of All Calibration Error Amounts	Average Absolute Value-Percentage of Accuracy Goal	Number of Error Amounts Exceeding Accuracy Goal	Highest Calibration Error - Ratio to Accuracy Goal
1-, 2-, and 5-degree Increments	29	12.7 arc-seconds	84.48%	10.6 arc-seconds	70.56%	6 of 29	2.09
5-degree Increments	18	11.4 arc-seconds	76.08%	8.7 arc-	58.08%	5 of 18	1.58

Readout Accuracy Results - Summary

Calibration Data Set	Number of Data Points Recorded *	RMS Value of All Readout Error Amounts	RMS Value - Percentage of Accuracy Goal	Average Absolute Value of All Readout Error Amounts	Average Absolute Value-Percentage of Accuracy Goal	Number of Readout Error Amounts Exceeding Accuracy Goal	Highest Readout Error - Ratio to Accuracy Goal
1-, 2-, and 5-degree Increments	7	13.8 arc-seconds	91.92%	13.2 arc-seconds	88.32%	2 of 7	1.37
5-degree Increments	14	12.7 arc-seconds	84.72%	11.3 arc-seconds	75.35%	5 of 14	1.32

* Data points were recorded as a ten revolution average of C_1 counts and $C_1 + C_2$ counts.

rms value of all error amounts calculated during pattern calibration was 12.7 arc-seconds for the schedule employing 1-degree, 2-degree, and 5-degree increments of data; the rms error value was 11.4 arc-seconds when using only 5-degree increments of test data. The lesser calibration error associated with only using the 5-degree increment data was unexpected. This result may be the result of having gathered all 5-degree increment data in one recording sequence of approximately one-half hour. The one- and two-degree increment data was recorded in subsequent runs; the total period of test data gathering encompassed about three hours. The abnormally high drift rate and rundown rate of this particular gyro will not occur again; the high rates were due to a processing oversight. The possible effects of error in compensating for gyro drift effects over the full set of calibration data versus one interior scan may account for the small difference in rms values of calibration error. As seen in Table 4, the average values of absolute error amounts exhibit the same overall relationship; i.e., the error content associated with the 5-degree increment schedule is the smaller of the two. All rms and average values compare favorably with the 15 arc-second goal for the program. The last column in the table shows the ratio of the highest single error value to the 15 arc-second goal.

After calibrating the pattern, the deviation of each remaining readout data point was computed with respect to the compensated pattern line. Most of these readout accuracy data points were taken near the pattern extremity where the greatest error is expected. More readout test values exist relative to the 5-degree increment calibration schedule because fewer points of the total recorded were using in the particular calibration. The rms value of error in reading out the several test attitudes of the gyro was 13.8 arc-seconds and 11.3 arc-seconds for the two calibration schedules. Again, all rms and average values of readout error are less than the 15 arc-second goal for the program.

The relatively small software program that was used to compensate the pattern and to deliver the stated readout accuracy of 13.8 arc-seconds (rms) has been measured in terms of it being stored and executed in a small, low power computer for space applications. The Honeywell HDC-301 Digital Computer was selected to provide a basis for the time and memory analysis. The computer has a basic word length of 16 bits with double precision capability; a typical core memory of 8k bits was considered. With data from each of two pickoffs processed into the direction cosines of attitude determination, this represents only a 3.6 percent load on the machine.

Appendix A

FLEXOWRITER DATA FORMAT

Readout and pattern calibration data was collected by means of the UG 1989A1 Data Processor which contains the logic, switching and accessory equipment necessary to read and record data from the Strapdown Electrically Suspended Gyro.

A portion of the data recorded as part of the gyro readout test is reproduced in this appendix (Table A-1); this portion consists of data taken in five degree increments input through the spindle axis of the test station dividing head.

Time is recorded in 0.0002-hour intervals. For example, the time of the first data line should be read as 2.1538 hours; the second line was read 0.0002 hour later at 2.1540 hours.

Data Group	Comments
1	Both No. 2 and No. 3 pickoffs are "looking" nearly at the rotor equator; their C_1 count totals are nearly the same. The rotor is running at about 244 revolutions per second as converted from the last column. The rotor is running down in speed throughout the test; this is observed in the continuously increasing count for the rotor period.
2	The dividing head has been moved by an increment of five degrees; the gyro case (and the array of three pickoffs) has been aligned relative to the dividing head so that pickoff No. 2 can be moved across the pattern according to the input angular change while pickoff No. 3 remains approximately static with respect to the pattern. The C_1 count for pickoff No. 2 has decreased; this indicates a shorter initial pattern interval.

Data Group	Comments
3 through 10	The spindle axis of the dividing head has been moved in five degree increments before each data group was enabled; the pattern has been read over a span of 45 degrees (5-degree increments times 9 readings) from the starting point near the equator.
11	The dividing head has been returned to its starting angle; the C_1 counts for both pickoffs No. 2 and No. 3 are again nearly equal. Because of rotor rundown, their absolute value in terms of counter sums are higher compared to the first data group. This data group provides the means of making a drift correction for the data recorded.
12	The dividing head spindle has been rotated five degrees from the selected starting reference angle; pickoff No. 2 is being moved in the opposite direction across the rotor pattern compared to that data gathered in data groups 1 through 11.
13 through 19	The spindle axis of the dividing head has been moved in five degree increments before each data group was enabled; the pattern has been read over a span of 40 degrees (5-degree increments times 8 readings) from the starting point near the equator. The small starting angle, offset from the equator, precluded reading out data at 45 degrees angular displacement as was done on the "other half" of the rotor.
20	The dividing head has been returned to its starting angle. This data group along with group 11 provides the means for calculating the draft correction for this latitude range of readout data.

TABLE A-1. FLEXOWRITER OUTPUT

Data Group	Time	Ten Rotor Revolution Counter Sums Accumulated Over First Pattern Interval (C_1) Pickoff No. 1	Pickoff No. 2	Pickoff No. 3	Run No.	Ten Rotor Revolution Counter Sum Rotor Period ($C_1 + C_2$)
	0215380	0000000	2095557	2101656	0000003	4104350
	0215400	0000000	2095637	2101767	0000003	4104524
1	0215420	0000000	2095715	2101893	0000003	4104667
	0215440	0000000	2095793	2101880	0000003	4104850
	0215460	0000000	2095883	2102079	0000003	4105019
	0215840	0000000	2020328	2103873	0000004	4108144
	0215860	0000000	2020416	2103905	0000004	4108312
2	0215880	0000000	2020483	2104013	0000004	4108480
	0215900	0000000	2020537	2104031	0000004	4108637
	0215920	0000000	2020707	2104239	0000004	4108821
	0216200	0000000	1943419	2105511	0000004	4111123
	0216220	0000000	1943509	2105640	0000004	4111258
3	0216240	0000000	1943570	2105629	0000004	4111465
	0216260	0000000	1943693	2105782	0000004	4111624
	0216280	0000000	1943716	2105849	0000004	4111779
	0216540	0000000	1863672	2107166	0000004	4113946
	0216560	0000000	1863744	2107192	0000004	4114126
4	0216580	0000000	1863826	2107264	0000004	4114285
	0216600	0000000	1863842	2107410	0000004	4114450
	0216620	0000000	1863939	2107442	0000004	4114622
	0216960	0000000	1779886	2109066	0000004	4117455
	0216980	0000000	1779933	2109203	0000004	4117609
5	0217000	0000000	1779997	2109328	0000004	4117791
	0217020	0000000	1780080	2109384	0000004	4117949
	0217040	0000000	1780140	2109432	0000004	4118095
	0217260	0000000	1688739	2110547	0000004	4119941
	0217280	000000	1688779	2110592	0000004	4120093
6	0217300	0000000	1688834	2110688	0000004	4120296
	0217320	0000000	1688903	2110747	0000004	4120454
	0217340	0000000	1688929	2110909	0000004	4120617

TABLE A-1. FLEXOWRITER OUTPUT (Continued)

Data Group	Time	Ten Rotor Revolution Counter Sums Accumulated Over First Pattern Interval (C_1) Pickoff No. 1	Pickoff No. 2	Pickoff No. 3	Run No.	Ten Rotor Revolution Counter Sum Rotor Period ($C_1 + C_2$)
	0217580	0000000	1587460	2112103	0000004	4122616
	0217600	0000000	1587454	2112266	0000004	4122773
7	0217620	0000000	1587519	2112297	0000004	4122967
	0217640	0000000	1587648	2112339	0000004	4123149
	0217660	0000000	1587670	2112438	0000004	4123306
	0218080	0000000	1472633	2114409	0000004	4126814
	0218100	0000000	1472644	2114528	0000004	4126962
8	0218120	0000000	1472619	2114660	0000004	4127143
	0218140	0000000	1472732	2114739	0000004	4127280
	0218160	0000000	1472676	2114859	0000004	4127462
	021850	0000000	1335791	2116521	0000004	4130458
	0218540	0000000	1335850	2116607	0000004	4130665
9	0218560	0000000	1335910	2116718	0000004	4130802
	0218580	0000000	1336060	2116781	0000004	4130962
	0218600	0000000	1336055	2116881	0000004	4131145
	0218860	0000000	1163740	2118123	0000004	4133276
	0218880	0000000	1163910	2118211	0000004	4133456
10	0218900	0000000	1164017	2118342	0000004	4133556
	0218920	0000000	1163986	2118415	0000004	4133845
	0218940	0000000	1164097	2118470	0000004	4134010
	0220040	0000000	2114855	2122675	0000005	4142878
	022006	0000000	2114933	2122840	0000005	4143061
11	0220080	0000000	2115025	2122981	0000005	4143220
	0220100	0000000	2115075	2123087	0000005	4143377
	0220120	0000000	2115122	2123134	0000005	4143525
	022046	0000000	2194855	2124521	0000005	4146234
	0220480	0000000	2195014	2124576	0000005	4146403
12	0220500	0000000	2195088	2124693	0000005	4146548
	0220520	0000000	2195147	2124757	0000005	4146744
	0220540	0000000	2195226	2124995	0000005	4146874
	0220880	0000000	2277065	2126264	0000005	4149560
	0220900	0000000	2277222	2126331	0000005	4149722
13	0220920	0000000	2277310	2126402	0000005	4149877
	0220940	0000000	2277413	2126516	0000005	4150040
	0220960	0000000	2277413	2126592	0000005	4150193

TABLE A-1. FLEXOWRITER OUTPUT (Continued)

Data Group	Time	Ten Rotor Revolution Counter Sums Accumulated Over First Pattern Interval (C_1) Pickoff No. 1	Pickoff No. 2	Pickoff No. 3	Run No.	Ten Rotor Revolution Counter Sum Rotor Period ($C_1 + C_2$)
	0221280	0000000	2362759	2127883	0000005	4152704
	0221300	0000000	2362853	2128024	0000005	4152876
14	0221320	0000000	2362961	2128057	0000005	4153016
	0221340	0000000	2363018	2128063	0000005	4153162
	0221360	0000000	2363114	2128283	0000005	4153297
	0221700	0000000	2454521	2129609	0000005	4155964
	0221720	0000000	2454608	2129700	0000005	4156103
15	0221740	0000000	2454660	2129813	0000005	4156266
	0221760	0000000	2454786	2129897	0000005	4156430
	0221780	0000000	2454816	2129950	0000005	4156585
	0222080	0000000	2554472	2131126	0000005	4158907
	0222100	0000000	2554613	2131249	0000005	4159040
16	0222120	0000000	2554695	2131288	0000005	4159169
	0222140	0000000	2554758	2131449	0000005	4159309
	0222160	0000000	2554862	2131527	0000005	4159480
	0222440	0000000	2666488	2132556	0000005	4161602
	0222460	0000000	2666635	2132702	0000005	4161763
17	0222480	0000000	2666652	2132769	0000005	4161922
	022250	0000000	2666821	2132833	0000005	4162070
	0222520	0000000	2666896	2132834	0000005	4162190
	0222760	0000000	2795456	2133922	0000005	4164045
	0222780	0000000	2795534	2134111	0000005	4164164
18	0222800	0000000	2795535	2134043	0000005	4164325
	0222820	0000000	2795668	2134143	0000005	4164446
	0222840	0000000	2795708	2134328	0000005	4164617
	0223080	0000000	2951187	2135189	0000005	4166421
	022300	0000000	2951539	2135187	0000005	4166471
19	0223120	0000000	2951473	2135268	0000005	4166692
	0223140	0000000	2951539	2135473	0000005	4166803
	0223160	0000000	2951828	2135530	0000005	4166989
	0224020	0000000	2130209	2139185	0000005	4173467
	0224040	0000000	2130294	2139332	0000005	4173589
20	0224060	0000000	2130405	2139428	0000005	4173776
	0224080	0000000	2130482	2139579	0000005	4173931
	0224100	0000000	2130527	2139613	0000005	4174104

Appendix B

COMPUTER FORMAT OF CALIBRATION AND READOUT DATA

The computer program written for the purpose of calibrating the pattern mechanization polynomial coefficients has in its output format tables of calibration and readout errors. Two calibration tables are reproduced below; Table B-1 is the result of calibrating over readout data points separated by five-degree increments, and Table B-2 is based upon calibration over readout data points separated by one-, two- or five-degree increments. This is the same data from which the pattern calibration results were calculated. The column headings used in the tables are:

Colatitude - The angular measure between the No. 2 pickoff line of sight and the rotor spin axis.

Count Ratio - Ratio of the time interval between passage of the pattern lines to the time interval for one full revolution of the rotor.

Compensated Colatitude - Each data point, initially listed according to its count ratio in column two, has been adjusted according to the compensation curve which was computed upon the entire set of calibration data points.

Calibration Error - This is the error in degrees between the measured colatitude angle listed in column one and the compensated colatitude angle in column three.

TABLE B-1. PATTERN CALIBRATION - FIVE-DEGREE INCREMENTS

Colatitude	Count Ratio	Compensated Colatitude	Calibration Error (degrees)
135,41317	,28161500	135,41313	-,00005
130,41138	,32340730	130,41209	,00070
125,40906	,35682420	125,40696	-,00210
120,40644	,38505080	120,41023	,00379
115,40474	,40988390	115,40038	-,00436
110,40316	,43227350	110,40177	-,00138
105,40094	,45300800	105,40752	,00658
100,39915	,47272400	100,39760	-,00155
95,39275	,49178640	95,39200	-,00075
90,39483	,51056749	90,39461	-,00022
85,42084	,52937029	85,42033	-,00051
80,42230	,54875930	80,41677	-,00553
75,42368	,56897049	75,42813	,00445
70,42514	,59059639	70,42826	,00312
65,42645	,61422630	65,42719	,00074
60,42770	,64073920	60,42245	-,00525
55,42881	,67131740	55,43125	,00244
50,42992	,70836169	50,42978	-,00014

Having computed a calibration curve based upon input data, the computer program can then accept additional readout data points which are not in the calibration set. The count ratio is used to calculate the compensated readout angle according to the calibration curve previously established. The program then compares the compensated readout angle to the colatitude input angle. Two tables of readout data are reproduced in this appendix (Tables B-3 and B-4). The headings used in these tables are:

Colatitude - This is the same angular measure between the No. 2 pickoff line-of-sight and the rotor spin axis, but all entries represent new data points not used in the calibration set.

Count Ratio - This is the output read from the gyro through the data processor at each of the colatitude angles listed in column one.

Compensated Readout - Each data point has been adjusted according to the readout compensation curve which was computed during the prior calibration process.

Readout Error - This is the error in degrees between the colatitude angle listed in column one and the compensated readout angle in column three.

TABLE B-4. READOUT ACCURACY RESULTS
BASED UPON PATTERN CALIBRATION
OVER FIVE-DEGREE INCREMENTS

Colatitude	Count Ratio	Compensated Readout	Readout Error (degrees)
135.06151	.28499010	135.05867	-.00264
134.05692	.29407200	134.06241	.00549
133.05292	.30273260	133.05371	.00080
132.04861	.31087010	132.05367	.00506
131.04431	.31866650	131.04741	.00309
130.04001	.32611840	130.04070	.00069
127.99412	.34032000	127.99700	.00288
125.99058	.35321980	125.99292	.00233
121.98493	.37661530	121.98058	-.00435
56.02575	.66742899	56.02123	-.00452
54.02871	.68095300	54.02351	-.00520
52.03171	.69559800	52.02872	-.00309
50.08656	.71124110	50.08692	.00036
49.09008	.71991900	49.09357	.00349